

## **Point-to-point to comments on se-2021-75**

Reply to Referee #2 and editors on "GPR signature of Quaternary faulting: a study from the Mt. Pollino region, southern Apennines, Italy" by Maurizio Ercoli et al., Solid Earth Discuss., <https://doi.org/10.5194/se-2021-75>, 2021

---

### **To: referee #2 and editors**

Dear all,

we really thank you for your final revision and for accepting our manuscript for publication. We here provide our answers to your requests.

Thank you,

Maurizio Ercoli, Daniele Cirillo and co-authors.

### **To: referee2**

In my opinion the revised version of the manuscript is substantially improved in text and figures and ready to be accepted for publication. Below few minor additional suggestions/comments.

Dear #referee2,

Again, thank you for your positive comments. We are glad that the changes applied to our manuscript now fits with your requests and suggestions.

We have applied also some minor corrections, as requested.

Best regards,

Maurizio Ercoli, Daniele Cirillo and co-authors.

---

REV#2:

Page 12 line 37: check the sentence sound, I suggest to change in: "But in cases like the VCT, the GPR data assume a key-value since provided key fault parameters where no direct information on the nature of the surveyed deposits and no accurate dating is available"

Authors: corrected

REV#2:

Page 13 line 1: I do not think GPR technique will never directly extract date for single event: dating of an earthquake (absolute but even relative) requires sampling of the stratigraphy at different levels.

Authors: we agree, thus we removed “currently” and we have rewritten the sentences 35-36 of page 12.

## **To: referee #2 and editors**

TE:

I have a couple of final remarks, which I would like you to take into account:

Lines 22-23: The sentence is hard to read, possibly split - "Pseudo-3D GPR data are harder to interpret, as they require to link geophysical features among different radar images. However, their use enabled the reconstruction of a reliable..."

Line 24: Rewrite more simply - "Our contribution better characterizes active faults in an area which falls within the Pollino seismic gap and is considered prone to severe surface faulting."

Line 26: The sentence remains unclear, try: "Our results are a constraint for further research at the study site while our approach and workflow are ideal for similar regions characterized by high seismic hazard and scarcity of near-surface geophysical data."

Authors: we have modified the sentences in the abstracts following the comments and rewriting the text.

Authors: Dear editors, finally, we would like to add also Dr. Daniele Cirillo (second contact) also as a second corresponding author, as he made an equal part of work for the writing and revision of this paper.

# GPR signature of Quaternary faulting: A study from the Mt. Pollino region, southern Apennines, Italy.

Maurizio Ercoli<sup>1-4</sup>, Daniele Cirillo<sup>2-4</sup>, Cristina Pauselli<sup>1-4</sup>, Harry M. Jol<sup>3</sup>, Francesco Brozzetti<sup>2-4</sup>

<sup>1</sup>: Università degli Studi di Perugia, Dipartimento di Fisica e Geologia, Piazza dell'Università 1, 06123 Perugia, Italy.  
<sup>2</sup>: Università degli Studi "G. d'Annunzio" di Chieti-Pescara, DiSPUTer, via dei Vestini 31, 66100 Chieti, Italy.  
<sup>3</sup>: University of Wisconsin - Eau Claire, Department of Geography and Anthropology, 105 Garfield Avenue, Eau Claire, WI, 54702.  
<sup>4</sup>: CRUST Centro interUniversitario per l'analisi SismoTettonica tridimensionale, Italy.

Correspondence to: Maurizio Ercoli ([maurizio.ercoli@unipg.it](mailto:maurizio.ercoli@unipg.it)) and Daniele Cirillo ([daniele.cirillo@unich.it](mailto:daniele.cirillo@unich.it))

**Abstract.** With the aim of unveiling evidence of Late Quaternary faulting, a series of ground penetrating radar (GPR) profiles were acquired across the southern portion of the Fosso della Valle-Campotenesi normal fault (VCT) located at the Campotenesi continental basin (Mt. Pollino region), in the southern Apennines active extensional belt (Italy). A set of forty-nine 300 MHz and 500 MHz GPR profiles, traced nearly perpendicular to this normal fault, were acquired and carefully processed through a customized workflow. The data interpretation allowed us to reconstruct a pseudo-3D model depicting the boundary between the Mesozoic bedrock and the sedimentary fill of the basin, which were in close proximity to the fault. Once reviewing and defining the GPR signature of faulting, we interpret near-surface alluvial and colluvial sediments dislocated by a set of conjugate (W- and E-dipping) discontinuities that penetrate inside the underlying Triassic dolostones. Close to the contact between the continental deposits and the bedrock, some buried scarps which offset wedge-shaped deposits are interpreted as coseismic ruptures, subsequently sealed by later deposits. Our pseudo-3D GPR dataset represented a good trade-off between a dense 3D-GPR volume and conventional 2D data, which normally requires a higher degree of subjectivity during the interpretation. We have so reconstructed a reliable subsurface fault pattern, discriminating master faults and a series of secondary splays. This contribution better characterizes active Quaternary faults in an area which falls within the Pollino seismic gap and is considered prone to severe surface faulting. Our results encourage further research at the study site, whilst we advise our workflow ideal also for similar regions characterized by high seismic hazard and scarcity of near-surface geophysical data.

**Key-words:** ground penetrating radar (GPR); Image processing; Faults; Neotectonics; Palaeoseismology; Earthquake hazards.

## 1. Introduction

A “seismic gap” is an area surrounded by regions struck by large earthquakes in historical or recent times. Such earthquake-free areas are characterized by the presence of seismogenic faults, whose past activity or possible quiescence is inferred on the basis of morpho-structural and/or paleoseismological data. The “seismic gaps” (McCann et al., 1979) show an apparent lack of historical seismicity but are candidate regions for the occurrence of large earthquakes in the near future (Mogi 1979; Plafker and Galloway 1989; Cinti et al., 1997; Galadini and Galli, 2003). A recent example of a seismic gap “filled” by strong earthquakes is the Mt. Vettore area (central Apennines) during

Deleted: ; [maurizio.ercoli@gmail.com](mailto:maurizio.ercoli@gmail.com).  
Formatted: Underline, Font color: Auto

Deleted: Although the use of pseudo-3D GPR data implies more complexity linking the geophysical features among the radar images,  
Deleted: w  
Deleted: ed  
Deleted: We believe our contribution provides an improvement in the characterization of active faults in the study area which falls within the Pollino seismic gap and is considered potentially prone to severe surface faulting  
Deleted: .  
Deleted: Our aim is for our approach and workflow to be of inspiration for further research in the study site as well as for similar high seismic hazard regions characterized by scarcity of near-surface geophysical data

Deleted: ,  
Deleted: ,

the 2016-2017 seismic sequence (Chiaraluce et al., 2017; Barchi et al., 2021 and references therein). Following the extensive coseismic ruptures mainly generated by the  $M_w = 6.5$  “Norcia” mainshock (Villani et al., 2018; Brozzetti et al., 2019; Testa et al., 2019), this area is currently an ideal laboratory for many conventional and innovative geoscience disciplines and applications (e.g. Xu et al., 2017; Porreca et al., 2018; Brozzetti et al., 2020; Cirillo, 2020; Ferrario et al., 2018; Ercoli et al., 2020; Michele et al., 2020; Porreca et al., 2020; Buttinelli et al., 2021; Ferrarini et al., 2021; Pucci et al., 2021; Sapia et al., 2021; Villani et al., 2021). In fact, although the area being characterized by a complex alignment of normal faults, no important earthquakes were reported over the past ~1500 years before this seismic crisis (Cinti et al., 2019; Galli et al., 2019; Galli, 2020). Former geological and geomorphological studies suggested the possible occurrence of Quaternary faulting (Calamita et al., 1992; Brozzetti and Lavecchia 1994; Barchi et al., 2000), which was successively confirmed by paleoseismological (Galadini and Galli, 2003) and GPR surveying (Ercoli et al., 2013a; 2014). These studies revealed the occurrence of strong paleo-earthquakes and suggested that the Mt. Vettore master fault was “silent” but prone to cause future seismic events. However, invasive trenching due to complex logistics, environmental restrictions, high costs and the need for authorizations, cannot be applied systematically in many locations. Thus, Quaternary faults and associated basins characterized by an unsatisfactory definition of the seismotectonic framework have to be investigated with geophysical techniques. For all the above noted reasons, and since the Mt. Vettore case may represent an analogue of similar seismic gaps, the southernmost Apennines were studied through a dedicated research programme (Agreement INGV-DPC 2012-2013 and 2014-2015, Project S1 - Base-knowledge improvement for assessing the seismogenic potential of Italy, Brozzetti et al., 2015; Pauselli et al., 2015) aiming to improve the knowledge-base of seismogenic structures. In the research, focused also on the Calabrian region (Southern Italy) during the 2012-2015 period, structural geology, geophysical, and paleoseismological data were successfully acquired on the Mt. Pollino and Castrovallari fault systems (northern Calabria), providing evidence of Late Quaternary activity (Ercoli et al., 2013b; Cinti et al., 2015; Ercoli et al., 2015; Brozzetti et al., 2017b). This area, which is considered one of the most important seismic gaps in southern Italy, extends from the Mercure basin to the north until Campotenese basin and Castrovallari plain to the south, all characterized by Late Quaternary continental syn-tectonic sedimentation (Fig. 1a-c).

The paleoseismological trenching and radiocarbon dating document in the region the occurrence of paleo-earthquakes with  $6.5 < M_w < 7.0$  and a recurrence time interval of ~1200 years (Cinti et al., 1997, 2002, 2015a,b; Michetti et al., 1997, 2000). But this high magnitude interval contrasts with the historical seismicity records, reporting a single significant  $M_w$  5.2 event occurred in 1693 (Tertulliani and Cucci, 2014). In the last three decade's instrumental seismicity recorded only two moderate seismic sequences climaxed in the  $M_w$  5.6 Mercure (1998, September 9) and  $M_w$  5.2 Mormanno (2012, October 25) earthquakes. The latter occurred during a long-lasting sequence spanning the period 2010-2014, which included more than 6000 seismic events of  $M_w > 1$  and activated at least three individual seismogenic sources (Passarelli et al., 2015; Brozzetti et al., 2017a, Fig. 1b). The gap between the low energy release, observed during the instrumented seismic sequences, and the high seismic potential estimated for the Quaternary faults, raised the question of whether even stronger earthquakes had shaken and could shake the area in the future. A recent and detailed parameterization of the Fosso della Valle-Campotenese fault (VCT in Fig. 1c) based on geo-structural and geomorphological mapping (Brozzetti et al., 2017a) as well as on seismological evidence (Totaro et al., 2014, 2015; Cirillo et., 2021), assesses a surface length of 15 km and a depth of at least ~10 km: the potential rupture-area is likely estimated to produce  $M_w > 6.0$  earthquakes. As testified by earthquakes of the last century, such magnitudes, in the Apennines extensional belt generally produce coseismic surface faulting (e.g. Oddone, 1915; Pantosti and Valensise, 1990; Boncio et al., 2010; Brozzetti et al., 2019). However, Quaternary faulting for the VCT

Deleted:

Deleted: ,

1 structure is currently unclear, but geological and morpho-structural data suggest this fault has played an important role  
 2 in determining the geometry and the recent sedimentary evolution of the basin.

3 The Campotenese basin and its VCT boundary fault is an example that summarizes the aforementioned issues: 1) lack  
 4 of availability of paleoseismological data as the basin is entirely located within the Mt. Pollino National Park, thus  
 5 requiring prior authorization from authorities; 2) lack of availability of publically accessible geophysical data; 3) no  
 6 fresh recent surface displacements within the Holocene deposits have been observed along its trace. For all these  
 7 reasons, the VCT represents an ideal case study suitable to test our working method.

8 We have conducted an explorative GPR field campaign across a VCT sector, suggested by discontinuous and smooth  
 9 geomorphic scarps, as a screening tool for the definition of its possible Quaternary displacement history. The  
 10 objectives of the paper are to: i) review and describe geophysical characteristics associated with a peculiar GPR  
 11 signature of faulting, and propose a reference methodological workflow; ii) specifically check the efficiency of GPR  
 12 prospecting to locate the VCT fault and to depict its subsurface pattern and spatial continuity at shallow depth; iii)  
 13 provide new data to eventually relate the occurrence of  $M_w > 6.0$  seismic events; iv) pave the way for other local  
 14 geophysical studies and identify interesting sites for future ground-truthing and/or paleoseismological trenching; v) to  
 15 have direct application and impact to the planning of future mitigation strategies for the reduction of surface faulting  
 16 risk in the nearby urbanized areas.

## 17 2. Tectonic setting and seismicity

18 The Campotenese continental basin is located in the northernmost Calabria region south-west of the Mt. Pollino  
 19 calcareous massif (southern Italy, Fig. 1). The bedrock of the basin consists of shallow water dolostones and  
 20 limestones, Late Triassic to Middle Miocene in age, belonging to the Verbicaro tectonic unit (Ogniben, 1969; Amodio  
 21 Morelli et al., 1976). It is generally referred to the western edge of the “Apenninic Platform”, a thick ( $> 4$  km)  
 22 carbonate shelf, that underwent compression during the Middle-Late Miocene times and was translated over an eastern  
 23 basinal domain (Lagronegro-Molise basin; Patacca and Scandone, 2007; Vezzani et al., 2010 and references therein).  
 24 From the bottom to the top, the bedrock succession includes late Triassic dolostones, Cretaceous limestones, and  
 25 Paleocene-Lower Miocene calcarenites cross-cut by the pillow lava basalts belonging to Liguride units of the  
 26 northern sector of Calabrian arc (Quitow, 1935; Grandjaquet and Grandjaquet, 1962; Amodio Morelli et al., 1976;  
 27 Ghisetti and Vezzani, 1983; Iannace et al., 2004, 2005 and 2007; Liberi et al., 2006; Filice et al., 2015; Tangari et al.,  
 28 2018).

29 The origin of the Campotenese basin, however, is related to a set of NW-SE striking extensional faults which, during  
 30 the Middle-Late Pleistocene, displaced the contractional tectonic pile, favoring the deposition of alluvial and lacustrine  
 31 sediments in a subsiding intra-mountain depression (Servizio Geologico d'Italia 1970). This set of conjugate SW- and  
 32 NE-dipping normal faults represents the local expression of the Quaternary extensional belt that develops all along  
 33 the Italian peninsula, nearly parallel to the axial zone of the Apennines, from northern Tuscany to the Calabrian Arc  
 34 (Brozzetti 2011). North of Campotenese, (Lucania and southern Campania) the Apennine extensional belt includes  
 35 several continental basins and their boundary faults, as the Irpinia, Vallo di Diano, Tanagro, Melandro-Pergola and  
 36 Val d'Agri (Ascione et al., 1992; Maschio et al., 2005; Amicucci et al., 2008; Villani and Pierdominici, 2010;  
 37 Brozzetti, 2011; Filice and Seeber, 2019; Bello et al., 2021). To the south, it continues with the Crati graben that  
 38 dissects the northern sector of the Calabrian Arc (Tortorici et al., 1995; Brozzetti et al., 2017b).

Deleted: ,

Deleted: ,

Deleted: ,

Deleted: and

Deleted: and

On the regional scale, the Quaternary normal fault array controls the release of major seismicity, as suggested by the distribution of supra-crustal instrumental earthquakes (INGV, 2020 and ISIDE, 2007) and of the strongest historical events (Fig. 1a, Tertulliani and Cucci, 2014; Rovida et al., 2020). The recent seismic activity as well as paleo-seismological investigations claim that most of the faults bounding the Quaternary basins are seismogenic and therefore enable, in some cases, to associate major past earthquakes with specific structures (e.g. Pantosti and Valensise, 1990; Cello et al., 2003; Spina et al., 2009; Brozzetti et al., 2009; Villani and Pierdominici, 2010). These same studies highlight that the kinematics of the Quaternary faults and the focal mechanisms of the major earthquakes are mutually consistent and are mainly compatible with an SW-NE direction of extension (RCMT and TDMT databases by Pondrelli, 2006 and Scogliamiglio et al., 2006). Other authors have recognized in the surrounding regions an oblique normal-lateral faults kinematics (e.g. Rossano and Sybaris faults, Galadini et al., 2001; Cinti et al., 2015b). The fault investigated in this work has been pointed out in more detail by Brozzetti et al. (2017a) in the frame of a larger study focussed on the Quaternary and active faults at the Calabrian-Lucanian boundary (Fig. 1a). In the region, three main sets of normal faults, with prevailing dip-slip kinematics, have been mapped: a western one, consisting of E- to NNE-dipping faults (red lines in Fig. 1b), and two other main sets of W-to SW-dipping fault segments (dark-blue and blue lines in Fig.1b). The Rotonda-Campotenese Set (ROCS) is a right-stepping en-échelon master fault developed for a total length of 15 km with an average N160E strike (blue, yellow rimmed lines in Fig.1b). ROCS is composed by two fault segments: i) the westernmost Fosso della Valle-Campotenese fault (VCT), which extends from the southern border of the Mercure basin to the SW boundary of the Campotenese basin, and ii) the Rotonda-Sambucoso fault (RSB), which branches-out from the VCT segment in the central part of the ROCS. In the northern sector, the two segments are averagely spaced ~ 2.5 km at surface and linked at a depth of ~ 9-10 km (Cirillo et al., 2021), cross-cutting the middle-Pleistocene ~ E-W striking Cozzo Vardo-Cozzo Nisco fault (CVN, light-blue line in Fig. 1b). Along the E-side of the Campotenese basin, the VCT is generally buried by Holocene deposits, but its location can be inferred based on stratigraphic observations and geomorphic features, such as sharp ridge fronts, linear scarps, and slope breaks. The VCT controls the distribution and thickness of the clastic fill basin (Middle Pleistocene-Holocene in age, according to Schiattarella et al., 1994) that reaches the maximum thickness (~ 30 m) in the western sector (VCT hanging wall, see boreholes stratigraphy at <http://sgi2.isprambiente.it/mapviewer/>). The spatial relationships, at surface and depth, between the Quaternary fault segments and the hypocenters of the re-located 2010-2014 seismic events (Totaro et al., 2015; Brozzetti et al., 2017a; Napolitano et al., 2020, 2021; Pastori et al., 2021) suggest that the VCT is a good candidate as a seismogenic source for the Mw 5.2 (2012, October 25) Mormanno earthquake, as well as for strong paleo-events.

Deleted: and

FIGURE 1 HERE

### 3. Methodology

Ground penetrating radar (GPR) is a high-resolution geophysical method able to provide detailed images of the shallow sub-surface. This methodology is based on the recording of EM reflections, with operative frequencies for geoscience applications generally between 10 MHz and 1000 MHz, depending on the transmitting and receiving antennae. The GPR reflections rise from dielectric permittivity contrasts between the subsurface targets and the surrounding media, which in geological and archaeological applications typically correspond to geo-lithological changes or water content variations (Jol, 2009). In low conductivity materials (“low-loss”), the maximum investigation depth is generally comprised within few tens of meters (Davis and Annan, 1989). The latter is however controlled also

by the electrical conductivity, which for high values causes radar signal attenuation (Annan, 2001). The reflections are recorded as a function of the Two-Way-Travel time (TWT) propagation, and displayed as a 1D GPR trace. Several GPR traces displayed along a transect build-up a radar profile or “radargram”, that is the 2D representation of the GPR reflections, more commonly identified as the conventional GPR output. A GPR dataset may be provided also as a 3D volume, which has been common for 25+ years in research applications and recently more widespread due to a wider diffusion of commercial GPR instruments equipped with arrays of antennae. The GPR is used in many research and applied fields, such as geological, sedimentological, geomorphic, hydrogeological applications (Bristow and Jol, 2003; Jol, 2009), and also in archaeological and engineering studies (Conyers, 2016; Daniels, 2004; Goodman and Piro, 2013; Utsi, 2017). In active tectonic context, several 2D/3D GPR studies have already imaged buried tectonic structures. These studies have shown geophysical images of faulting, supporting and/or extending outcrop, borehole, trench data, and contributing to base-knowledge of seismogenic structures as well as to the seismic hazard assessment of several regions around the world. Among the pioneers, we can mention Benson (1995), Smith and Jol (1995), Busby and Merritt (1999), Cai et al. (1996) and Liner and Liner (1997), and on the successive twenty years, other 2D GPR studies were achieved across several faults worldwide (Audru et al., 2001; Demanet et al., 2001; Overgaard and Jakobsen, 2001; Bano et al., 2002; Liberty et al., 2003; Reiss et al., 2003; Slater and Niemi, 2003; Malik et al., 2007; Wallace et al., 2010; Yalciner et al., 2013; Imposa et al., 2015; Anchuela et al., 2016; Nobes et al., 2016; Matos et al., 2017; Pousse-Beltran et al., 2018; Zajc et al., 2018; Zhang et al., 2019 and Shaikh et al., 2020). In Italy, only a few GPR studies are currently available across normal faults (e.g. Salvi et al., 2003; Jewell and Bristow, 2006; Pauselli et al., 2010; Roberts et al., 2010; Ercoli et al., 2013a; 2014; Bubeck et al., 2015; Cinti et al., 2015). Over time, 2D GPR acquisitions were flanked by an increasing number of pseudo-3D or full-3D GPR studies (Grasmueck et al., 2005). Grasmueck and Green (1996) traced the future path of three-dimensional GPR applications, providing a dense 3D GPR volume to image fractures in a Swiss quarry. The study opened the possibility to three-dimensional GPR imaging of subsurface geological structures. Successive studies extended the approach to characterize active faults in different tectonic regimes combining 2D and pseudo-3D GPR surveys (e.g. Gross et al., 2002, 2003, 2004; Green et al., 2003; Tronicke et al., 2006; McClymont et al., 2008, 2009, 2010; Vanneste et al., 2008; Christie et al., 2009; Carpentier et al., 2012a,b; Malik et al., 2012; Brandes et al., 2018). A review of the near-surface GPR faulting studies suggests some reflection characteristics as possible indicators for the detection of subsurface fractures and faults (e.g. Smith and Jol, 1995; Liner and Liner, 1997; Reiss et al., 2003; Gross et al., 2004; McClymont et al., 2008, 2010 and Bubeck et al., 2015). Among these, sharp lateral reflectivity variations, interruptions of the reflections, and the presence of hyperbolic diffractions are considered convincing evidence, as shown also by numerical simulations (Ercoli et al., 2013a; Bricheva et al., 2021). In addition, we have accounted for additional GPR indicators identified for Quaternary faulting in similar environments (Ercoli et al., 2013a,b; 2014; 2015), which are linked to the geometry of stratigraphic deposits across fault zones: i) reflections abrupt truncating and offsetting along sub-vertical discontinuities (especially in the case of a normal fault); ii) reflection packages thickening as they approach the fault strands; iii) abrupt lateral dip variation of the reflections; iv) peculiar reflection package geometries, with contorted reflection patterns resembling “*colluvial wedges*”, which McCaipin (2009) defines as deposit due to “*subsidence and sedimentation of the hangingwall and erosion of the morphological scarp in the footwall*”; v) localized strong GPR signal attenuation due to the presence of conductive media within the main fault zone.

Based on the research and criteria reviewed above, we carried out a near-surface interpretation of faulting based on the co-existence of most of these features along several adjacents analyzed GPR profiles. These conditions strengthen

Deleted:

the interpretation of each profile and aids to highlight the spatial continuity of the interpreted structures over linear distances of at least many tens, or hundreds, of meters.

### 3.1 GPR and GNSS survey

Three different geophysical field campaigns carried-out during the 2014-2015 years, a dataset of 49 GPR profiles was acquired in the southern sector of the ROCS across the VCT fault segment (Fig. 1b-c), covering a buffer zone of ~ 400 m and ~ 200 m respectively along and across the fault strike (area of ~ 8 Ha), for a total linear length of GPR profile about 4100 m collected using a Common Offset (CO) configuration (Fig. 2).

FIGURE 2 HERE

We used a Zond 12e GPR system equipped with 300 and 500 MHz antennae. The lower frequency antennae was ultimately preferred and considered the best trade-off between maximum resolution and achievable signal penetration (in our case ~ 4 m) concerning the surveyed materials and wanted subsurface structures. The GPR was equipped with an odometer wheel to measure the radar profiles' length and with a Topcon GR-5 Global Navigation Satellite System (GNSS) receiver to achieve accurate positioning of GPR traces and profile. Considering the scarce presence of obstacles across the survey site and the good satellite coverage, we opted for a Network Real-Time Kinematic positioning (NRTK, connected to the NETGEO network), measuring coordinates and elevations with centimetre accuracy, and stored directly within the SEG-Y GPR files.

Three datasets were acquired after preliminary fieldwork and collection of geological structural data at the surface and which allowed us to infer the possible location of the fault trace. The average NE-SW direction of the GPR lines was initially planned with the primary purpose of intersecting the VCT fault ~perpendicularly to its SW-NE strike, as reported by literature and visible by surface evidence. This solution theoretically allows a more reliable interpretation of the investigated structure by reducing the effect of the apparent dip-direction and dip-angle of both stratifications and faults.

The acquisitions carried out in 2014, first resulted in twelve SW-NE GPR profiles collected in the southern sector of the basin (CMT light-blue lines in Fig. 2a), which was a flat land characterized by Quaternary alluvium. The second acquisition encompassed four additional radar profiles collected in the same area, and another nine radar profiles progressively moving to north, which were collected with slightly different and converging orientations in the central sector (CMT green lines Fig. 2a). This solution was pursued for two main reasons: 1) to avoid directly surveying the outcropping dolostones (only partially crossed with two northernmost profiles) characterizing two hills *h1* and *h2* (dashed white polygons in Fig. 2), and thus focussing only on the sedimentary cover which is our target for possible Quaternary faulting; 2) to optimize, through a preliminary GPR data interpretation, the future acquisition schemes by figuring out the dip direction of the buried geologic structures of interest. In fact, similarly to the interpretation of reflection seismic profiles, the "apparent dip" of reflections in bidimensional radar profiles should be considered to achieve a reliable 3D conceptual model.

In order to intercept several possible buried faults and fault-related structures as well as to fully image the local structural setting, the successive 2015 acquisition crossed part of the Triassic dolostones ridge with longer GPR profiles. The GPR profiles collected during the second 2014 campaign (close to *h1* and *h2*) already revealed a considerable difference in GPR reflectivity between the unconsolidated deposits and layered and fractured Mesozoic lithotypes (Gafarov et al., 2018). Therefore, two new datasets of 24 parallel GPR radar profiles (CMT dark-blue sets



of lines in Fig. 2a, *north “n”* and *south “s”*) were extended in NNE-SSW and NE-SW directions, respectively, crossing *h1* for several tens of meters (max profile length ~220 m) throughout the basin. The GPR profiles were recorded using a trace step of 0.05 m and a profile inter-distance of 25 m for dataset “*n*” and 10 m for dataset “*s*”, respectively. A detailed summary of the acquisition parameters used for the GPR surveys is reported in Table I. For these two datasets, the profile spacing and positioning are more regular and accurate, thanks to a preparatory transects planning using a GIS project. Thus, we later staked out their initial and final positions during the fieldwork through the differential Global Navigation Satellite System (GNSS). The results of the accurate GPR traces positioning achieved during the GNSS campaigns were also later used for GPR data processing, visualization, and interpretation.

TABLE 1 HERE

### 3.2 GPR data processing and results:

The processing sequence was customized after testing several workflows and parameters. We aimed to remove random and coherent (e.g. ringing) noise and enhance the data quality to better visualize the geometry of the buried reflections and their discontinuity in signal amplitude and phase. The first step was an accurate Quality Control (QC) of the profile coordinates and topographic profiles. Although the generally favorable environmental conditions (e.g. good satellite coverage, no forested areas etc..) of the site for a GNSS survey, some measurements were occasionally suffered a degradation of positional accuracy (e.g. temporary scarce satellite coverage or poor communication via Network Transport of RTCM via Internet Protocol - Ntrip). For some traces therefore the coordinates and elevation field records that were outliers (Fig. 3a) were corrected using various strategies (e.g. replacement, interpolation, or smoothing, Fig. 3b).

FIGURE 3 HERE

We have also compared our measurements with topographic transects extracted from a 10 m and a 5 m resolution Digital Terrain Models (DTM) by Tarquini et al. (2012) and by Regione Calabria. Later on, we finally used a 1 m resolution DTM (Geoportale Nazionale, Lidar data provided by Italian Ministero dell'Ambiente e della Tutela del Territorio e del Mare - MATTM) to double-check if, despite the different scales of observation, the topographic profiles were comparable. Although the metre resolution of the DTM is unable to represent centimetre topographic variations, the comparison confirmed an excellent match of the topographic profiles at a meter scale, so that the DTM data were integrated to correct the GNSS measured topography when the accuracy of GNSS recordings were excessively degraded. With the topographic profiles corrected, the raw GPR data (Fig. 3c, illustrating the profile cmt5s) were initially processed with the Prism software (Radar System, Inc., <http://www.radsys.lv/en/index/>) using a basic processing sequence, to analyze the main characteristics of data and optimize a customized processing flow. The processing sequence was later improved through ReflexW software (<https://www.sandmeier-geo.de/reflexw.html>, see Table II for details on the processing algorithms and parameters). The workflow included a time-zero correction, dewow, amplitude recovery, velocity analysis, background removal, bandpass filtering, F-K filtering, 2D time migration, topographic correction, and time-to-depth conversion. The amplitude recovery was operated through a “gain function” including a linear and an exponential coefficient ( $g(t) = (1+a*t)*e^{(b*t)}$ ) to enhance the amplitude (reflectivity) contrasts as well as preserving the horizontal and vertical amplitude variations already visible in the raw data (Fig. 3a). This amplitude recovery function was used across all the profiles with slight customization depending

on the datasets (details in table II). The entire processing flow was applied to all the available radar profiles, again with occasional filtering adaptations aiming to remove local pervasive signal ringing (e.g. due to low antennae-ground coupling). Particular care was dedicated to the migration process, whose algorithm was decided after extensive tests on several radar profiles to select the best migration strategy.

TABLE 2 HERE

In fact, a very different reflectivity and maximum depth of penetration are visible in the data: it is more than 150 ns in the central sector, reducing to 70-80 ns in the rest of the radar profiles (Fig. 3c): this fact suggests sharp lateral variations of subsurface media (Figs. 3d) and possibly of the velocity field. Thus, we have first tested a 1D time migration algorithm (Kirchhoff) performing a Migration Velocity Scan (MVS) analysis (Forte and Pipan 2017) and inspecting the success of diffraction hyperbola collapse after migration. We have varied constant values of EM velocity, from a minimum of 0.06 up to 0.12 m/ns, with steps of 0.01 m/ns, to evaluate considerable variation in dielectric properties of surveyed media. The MVS is characterized by a higher velocity for the central sector of the GPR profiles which displays high reflectivity: Fig. 4 illustrates an example of the migration results obtained on the profile cmtIn\_a, by using three constant values of average velocity. The profile in Fig. 4a shows the unmigrated version characterized by numerous hyperbolic and half hyperbolic diffractions originated by single scatter points and wavy reflections (white arrows). In Fig. 4b we display the first test using  $v = 0.07$  m/ns, showing overall good results, with slightly under-migration at a few points mainly located within the shallower sediments (light-blue arrows). The hyperbolic diffractions are also nicely collapsed using higher velocity ( $v = 0.09$  m/ns) as shown in Fig. 4c (dark-blue arrows), even if some imaging problems affect deeper reflections. The last migration scan test ( $v = 0.11$  m/ns) displays a good result only in few profile sectors (dark-blue arrows), particularly localized within the sectors with high reflectivity, displaying an improved lateral reflection continuity. The rest of the radar profiles show generally poor imaging, particularly in the area characterized by strong attenuation, where the wavy reflection is over-migrated (red arrows indicating migration smiles, Fig. 4d).

FIGURE 4 HERE

The workflow therefore, suggests a challenging imaging task due to velocity variation happening not only in depth as well as laterally across the different media. This sharp change of reflectivity and velocity at a distance of about 13-14 m (Fig. 4d) represents a complex problem for the efficiency of 1D migration algorithms standardly used for GPR imaging. Such considerations has lead testing a 2D migration algorithm, by creating and using a 2D velocity model obtained for each radar profile through a hyperbolic diffraction fitting tool (Fig. 5a). Single velocity points have been fitted for each area displaying hyperbolic diffractions, while in the remaining parts of the radar profiles we have arbitrarily included presumed velocity adaptation only to obtain a regular grid of points to spatially interpolate the 2D models. The 2D migrated radar profiles, in comparison to the 1D approach, resulted in improved imaging of GPR profiles, displaying a more accurate collapse of the hyperbolic diffractions into point sources and an improved relocation of dipping reflections, with a refinement of their geometry and an increase of their continuity. A good-quality imaging result is visible on the central sectors of radar profiles displaying strong reflectivity and reflections with improved continuity, but also many phase breaks and displacements. Despite steep topographic gradients, sharp lateral velocity variation and the reflection heterogeneity might cause imaging issues that need to be treated using more specific workflows (Lehmann and Green, 2000; Heincke et al., 2006; Goodman et al., 2007; Dujardin and Bano,

Deleted:

2013). We believe we have reached a good compromise for our purposes. In our case, a considerable improvement, can be seen along the hill-slope and flatter areas (profile cmt1n\_a, Fig. 5b) which are of greatest interest for the study aimed at detecting possible earthquake ruptures within the Quaternary deposits. The improved imaging of reflection geometries is therefore fundamental for the interpretation and detection of geophysical signatures of faults.

FIGURE 5 HERE

A successive import of the processed SEG-Y data was done into the seismic interpretation software OpendTect Pro v.6.4 (Academic license courtesy of dGB Earth Science, <https://www.dgbes.com>), which was used first for global quality control of processing operations (correctness of topographic correction and datum plane, coordinates accuracy and matching, profiles orientation and intersection) and for three-dimensional (3D) visualization of all the profiles (Fig. 6a). The three-dimensional GPR project was subsequently integrated with geological and structural maps, DTM, and literature schemes (using a common Coordinate Reference System: WGS84 UTM Zone 33N, EPSG: 32633) in the Move suite software v. 2019.1 (Academic license courtesy of Petroleum Experts, <https://www.petex.com/>) for GPR interpretation and model building. All the E and W-dipping fault surfaces were created interpolating the fault-sticks picked on displaced reflections and correlated across adjacent radar profiles. In particular, we used the "surface geometry" tool to extract the properties of each single mesh building up the surfaces, and obtaining the "dip" and "dip azimuth" data. Subsequently, such values have been automatically saved in an attribute table, which can then be queried to reconstruct the "synthetic" stereonet.

#### 4. GPR data description and interpretation

The 3D MOVE project allowed us to extract 2D and 3D data visualizations to better figure out the relationships between the main reflections identified on the different GPR profiles (Fig. 6a). The workflow aimed to reconstruct and model the three-dimensional surfaces including both horizons and high-angle discontinuities.

FIGURE 6 HERE

A common feature on all the radar profiles is the strong reflectivity visible within their central sectors (e.g., profile cmt3n in Fig. 6b), which are characterized by an irregular and steep slope, particularly within the northern portion of the surveyed area. These sectors show deep GPR signal penetration due to the Triassic dolostones, which outcrop in the central and northern portions of the study area (Figs. 1c and 2a). The quality of the radar reflections and the remarkable depth reached (~6 m, Fig. 6b) suggest this rock type is an excellent dielectric medium (corresponding to higher frequency content zone in the 2D spectrum of Fig. 6c). However, its reflection pattern is not spatially homogenous, being characterized by oblique and sub-parallel reflections. The latter are interpretable as dolostone beds of moderate (25-30°) W and E "apparent" dip on the respective sides of the surveyed dolostone hills. In addition, these reflections are frequently cut and slightly displaced by apparent high-angle (60-65°) phase discontinuities, highlighted by a dense hyperbolic diffractions pattern (radar profile cmt2n, Fig. 7a), suggesting intense fracturing and little faults displacing the dolostone (Fig. 7b). This radar signature was recorded not only in correspondence of the outcropping carbonate but also in the transition slope areas covered just by a thin soil layer (Figs. 7b,c). In the southern side of *h1*, an outcrop with thin microbialitic laminae allows one to measure the attitude of the bedding (NNW dip, ~30-35° dip

1 angle) as well as two sets of major and minor joints (SW and SE dip and dip angle of ~ 40-45°, respectively) fitting  
2 with GPR reflections.

3 Apart from its internal heterogeneities, the GPR signature of the Triassic dolostones can be considered as a well-  
4 defined depositional facies (*fc1*) (Sangree and Widmier, 1979; Huggenberger, 1993; Beres et al., 1999; Jol and  
5 Bristow, 2003). A different radar signature *fc2* is defined for the profile sectors on the sides of *fc1*. This second facies  
6 is characterized by prominent laterally-continuous and sub-parallel reflections in the very shallow depth range (< 1 m,  
7 just beneath the direct arrivals), stratigraphically sealing underlying reflections 1-3 m deep: the latter are more  
8 discontinuous, wavy, and contorted, with moderate to low reflectivity and encompassing sparse diffraction hyperbolas  
9 (in unmigrated data, Fig. 7a). This reflection pattern overlaps onto a generally prominent wavy reflection (Fig. 7a,b),  
10 which typically marks the transition to strong signal attenuation deeper in the section.

11

FIGURE 7 HERE

12 The reflection package belonging to *fc2* corresponds to the alluvial/colluvial deposits (Fig. 7b-d), outcropping on the  
13 sectors with flat topography, which represent the GPR profile sectors we've carefully inspected to find for geophysical  
14 evidence of Quaternary faulting. A key-layer for this research is the described prominent, wavy reflection, as it can  
15 be recognized in many radar profiles. The related interpretation is not straightforward in the absence of direct data  
16 (e.g. boreholes and/or paleoseismological trenches) or at least without additional geophysical data. A strong GPR  
17 reflection suggests significant variation of the dielectric constant between the two media so that most of the incident  
18 energy is reflected back to the receiver at the surface. This wave behaviour is potentially explained by several  
19 geological models, such as: i) a high dielectric contrast may be a result of a sharp soil moisture variation (Ercoli et al.,  
20 2018); ii) a sharp erosional, stratigraphic or tectonic boundary within heterogeneous deposits (Ercoli et al., 2015), or  
21 iii) a contact between two considerably different lithologies, such as unconsolidated deposits laying above a bedrock  
22 substrate reflecting back all (or almost all) the incident signal (e.g., Frigeri and Ercoli, 2020). In addition, the possible  
23 role of conductive deposits (e.g. high clay content) should not be discounted to explain the occurrence of strong  
24 attenuation. Several considerations are at the basis of the GPR data interpretation:

25 1) the available well logs show the Pleistocene-Holocene alluvium and colluvium layered above the carbonate bedrock  
26 ~20-30 m depth (Brozzetti et al., 2017a), a greater depth than the strong GPR reflection. However, it should be  
27 observed that the area drilled is located ~2.5 km away on the north-westernmost sector, over the depocenter of the  
28 Campotenesse basin, whereas the studied GPR site is placed just on its eastern border, in proximity to emerged  
29 dolostone hills; 2) only terraced Middle-Pleistocene silts and sands (Schiattarella et al., 1994) and slight coatings of  
30 Late Pleistocene colluvium (generally < 2 m thick) are documented to outcrop in the eastern sector of the basin  
31 (footwall of VCT fault) (see Fig. 7 in Brozzetti et al., 2017a); 3) the subsurface geometries highlighted by the  
32 prominent GPR reflection and underlying reflection pattern suggest a relatively thin layer of sedimentary deposits  
33 resting on a fractured substratum. Its top surface is progressively deepening towards the W, thus providing increased  
34 space for settling sediments and thus a gradual thickening of deposits is observed from E to W.

35 In light of the above considerations, we interpret the prominent, wavy GPR reflection as a buried top layer of carbonate  
36 (e.g. as observed e.g. by Bubeck et al., 2015), in our case represented by the Triassic dolostone formation. The latter  
37 is lying at a shallower depth (1-3 m) beneath shallow and poorly consolidated Quaternary deposits, across both sides  
38 of the surveyed hills. Thus, after picking such a prominent reflection event on all the radar profiles, the top of bedrock  
39 surface was reconstructed as shown in Fig. 8a (coloured surface). In this figure, we display also an overlay of a recent

Deleted:

Deleted: s

structural map of the basin (modified after Brozzetti et al., 2017a) reporting the area dissected by a set of en-echelon fault splays to the West associated to the VTC segment. Thus, analyzing the geophysical characteristics of the prominent, wavy reflection in terms of a structural interpretation, the main peculiar characteristic is the clear “stepped” geometry of some sectors (Figs. 5b, 6b, 7b, 8b), namely breaks of its continuity associated to lateral sharp variations of depth (linked to sediment growth and onlaps). We also notice other geophysical features, which can be observed in the stratigraphy of overlying deposits (*fc2*): some reflections are semi-continuous to discontinuous (sharp variation in signal amplitude and phase) and display evident lateral variation of the dip angle.

FIGURE 8 HERE

These broken reflection packages present truncations (e.g. Smith and Jol, 1995), displacements, and hyperbolic diffraction events (insets of Fig. 8b1,b2). Such peculiar GPR signature is therefore compatible with coseismic displacement due to Late Quaternary surface faulting events (Fig. 8b). Contorted reflections across the main discontinuities frequently show localized strong attenuation of GPR signal (Fig. 8b). The attenuation might be linked to their high dip-angle, causing a minor amount of energy being reflected back to the antenna, but, more likely, due to the presence of conductive fine soils nearby faulted zones (e.g. circle 1 in Fig. 8b). These conditions can be linked to different depositional facies across fault zones (McClymont et al., 2010) e.g. including colluvial wedges (Reiss et al., 2013; Bubeck et al., 2015) or deposits deriving from degradation of fault scarps (detailed interpretation within the caption of Fig. 8b). Using all such stratigraphic evidence and geophysical markers of faulting, we have therefore interpreted and classified synthetic (W-dipping, blue) and antithetic (E-dipping, red) normal faulting events (Fig. 8b). During the interpretation process, the faults were picked using solid lines (fault sticks); when the presence of geophysical markers of faulting were uncertain, a dashed fault segment was initially added and revised a second time their possible connection among nearby GPR profiles.

The interpreted faults present a dip angle between 65-75° and variable amount of displacement (*D*), estimated by correlating the position of the top of the carbonate substratum in the footwall and hanging wall blocks (e.g. scheme summarized in the inset of Fig. 8b3). Considering the GPR profile of Fig. 8 as representative for the studied VCT sector, *D* is not exceeding ~1 m for the W-dipping splays within the Quaternary sediments (~0.5 m for the E-dipping splay). A displacement *D* of ~1.5 m was derived across the sharp boundary between the Triassic dolostone and the Quaternary deposits (easternmost fault on Fig. 8b), being interpreted as the main fault. This clear contact is characterized in all profiles by hyperbolic diffractions (in unmigrated data), variable dip angle, abrupt truncations, sharp lateral variation of the reflectivity suggesting a wide fault zone (Figs. 3 to 9), controlling the above mentioned Quaternary splays. By interpolating all the fault sticks placed in adjacent profiles, we have created the fault surfaces, that show a good degree of continuity from north to south (Fig. 9). For the studied sector of the VCT, we have reconstructed the tridimensional fault-network and the geometry of the associated synsedimentary deposits at a metric scale of observation (Fig. 9).

5. Discussion

5.1 Inferences from subsurface 3D model

The perspective view of Fig. 9a shows a 3D structural scheme of the main tectonic lineaments at the basin scale displaying a NW-SE faults strike (modified after Brozzetti et al., 2017a) in relation to the GPR investigated area (white rectangle). Our GPR interpretation enriches many of the details such a former structural scheme across the southern VCT segment. We highlight an en-echelon system of two main SW and NE-dipping faults as well an articulated set of extensional meso-faults within the Quaternary sediments. The high-angle GPR discontinuities identified in the study (e.g., Fig. 9b) show a considerable continuity in the NW-SE direction (accurate 3D structural reconstruction in Fig. 9c), dissecting not only Quaternary alluvial-colluvial deposits (except for the very shallow *fc2* layers), but also deeper stratigraphic layers.

The reconstructed faults mark a horst-graben structure, mostly buried within the Campotenese basin, which locally emerges from the Quaternary deposits. In the investigated area it corresponds to a NNW-SSE elongated topographic high (*h1* and *h2* in Fig. 2a) made by the Triassic dolostone. This horst is bordered toward the W and towards the E by SW- and NE- dipping normal faults, respectively (Figs. 9b, c). In Fig. 9c, the fault-set *d1*, together with its antithetic set *d2*, shows the maximum displacement and the most evident deformation of the adjacent sub-surface deposits. The variations of thickness of such Quaternary deposits are consistent with the horst and graben configuration. Thinning is observed in correspondence with the raised buried blocks, whereas thickening, wedge-shaped as well as chaotic geometries correspond to the lowered blocks. The main fault of set *d1* can be considered a conjugate fault of the VCT (Fig. 8b), separated by a right step-over of about 0.5 km from the segment that borders the eastern basin (Figs. 2c, 8a). Thus, also the fault-set *d3* and *d4* located on the eastern part of *h1* and *h2*, can be hierarchically classified as a network of minor splays embedded in the southern junction zone between the two VCT segments (Fig. 9c).

The three-dimensional model (Fig. 9a,c) highlights that these faults, despite having a typical Apenninic NW-SE trend, are characterized by a complex polymodal pattern of strikes, with alternating N-S to NW-SE direction. Therefore, such a polymodal character which was observed along all the extensional structures of the area (Brozzetti et al., 2017a) is also confirmed at the GPR scale along this VCT sector. A dedicated statistical analysis of the reconstructed fault planes is reported in the stereo plots of Fig. 9d (*d1-d3*= W-dipping faults; *d2-d4*= E-dipping faults).

FIGURE 9 HERE

5.2 Seismic hazard implications

The combination of geological and seismological data may suggest outcropping Quaternary faults being capable of releasing earthquakes, but the determination of the maximum expected magnitude along these faults might not always be well constrained. An estimate can be made using well-known scale-relationships (Wells and Coppersmith, 1994; Wesnousky et al., 2008; Leonard, 2010; Stirling et al., 2013) with knowledge of the geometric parameters (e.g. fault length, area and depth), which are often difficult to assess. These scale relations can also be applied also to Quaternary scarps originated by cumulative coseismic faulting produced by medium-strong earthquakes (generally  $M > 6$ ). Nevertheless, only through paleoseismological analysis, by sampling and dating the stratigraphy at different levels, is it possible to date and distinguishing the amount of slip of each seismic event. But in cases like the VCT, the GPR data assume a key-value since provided key fault parameters where no direct information on the nature of the surveyed

Deleted: ,

Deleted: ,

Deleted: ,

Deleted: due to

deposits and no accurate dating is available. Our GPR interpretation by itself doesn't allow one to extract any date for a single earthquake, nor identify a succession of past seismic events and neither establish recurrence times (Galli, 2020). However, it confirms a segmentation of the VCT and the presence of buried splays, which appear to have exerted a strong control on the deposition of Late Quaternary sediments. The location of Quaternary ruptures at a shallow depth in a flat land of an intra-mountain basin presently undergoing alluvial and colluvial sedimentation, suggests their occurrence might be attributed to the Holocene. Thus, pointing out normal faulting of Holocene deposits would be, in itself, a very important and novel result for the Campotenese area. A Middle-Late Pleistocene age of activity was suggested for the Mercure and Campotenese boundary faults by Schiattarella et al. (1994) and Brozzetti et al. (2017a), with Holocene activity indirectly inferred on the base of morpho-structural observations. More recently, an earthquake-structure association with the recent 2010-2014 Pollino seismic sequence has been reconstructed through cross-sections and relocated seismicity in Cirillo et al., (2021).

Our data are promising because the GPR facies interpretation highlights the possible presence of small-scale grabens or half-graben (maximum estimated fault zone width of ~ 160-170 m, inset c1 of Fig.9c) and the likely fault-related deposits (e.g. as observed by Reiss et al., 2013 and Bubeck et al., 2015) at shallow depth. This inference would testify to not only the persistence of extensional deformations up to the Late Quaternary but would even imply the occurrence of episodes of surface faulting. In other words, the Campotenese basin may have been affected in the relatively recent past by medium-strong earthquakes, larger than the 2010-2014 mainshocks. It should be in fact considered that historical events with  $6 < M_w < 7$  surrounded the area, being documented a further ~ 50 km north (1857 -  $M_w$  7.1) and ~ 60 km south (1184 -  $M_w$  6.7, Fig. 1a) (Rovida et al., 2020). Some paleoseismological earthquakes with inferred magnitude  $6.5 < M_w < 7$  are attributed to the Castrovillari fault, located ~ 20 km SE and also falling within the Pollino seismic gap (Cinti et al., 1997; Michetti et al., 1997; Cinti et al., 2002, 2015).

The estimates of the VCT fault-length provide an overall value of 15 km (Brozzetti et al., 2017a) which is compatible, in the case of a complete rupture, with the maximum expected magnitudes of  $M_w = 6.45$  (Wells and Coppersmith, 1994) and  $M_w = 6.8$  (Wesnousky et al., 2008 and Leonard, 2010), therefore well capable to produce surface breaks. Being the source of the most recent earthquakes (2012 -  $M_w$  5.2; 1894 -  $M_w$  5.1; 1708 -  $M_w$  5.8 and perhaps 1693 -  $M_w$  5.2) affecting the study area estimated at ~ 8 km depth (Totaro et al., 2015; Brozzetti et al., 2017a; Napolitano et al., 2020, 2021; Sketsiou et al., 2021), the level of seismic energy released by such historical seismic events would likely be not enough to generate the VCT ruptures at surface. Therefore, it sounds reasonable that the hypothesis of past earthquakes occurrence, nucleated from the VCT, with a magnitude sufficiently high to cause the buried coseismic ruptures, highlighted by our GPR interpretation, which were then subsequently erased at surface by footwall erosion and sedimentation at the hanging wall. In addition, because historical catalogs do not show events with  $M_w > 6$  (Rovida et al., 2020), a very energetic earthquake could have likely occurred before the period covered by the available seismological catalogs, proving new perspectives on the actual seismic hazard of the area.

## 6. Conclusions

Our novel GPR data and dedicated workflow allowed us to obtain a detailed 3D model of the southern sector of the Fosso della Valle - Campotenese fault (VCT) in the continental Campotenese basin, a seismic gap in the Mt. Pollino region (Southern Italy). The processing, analysis, assemblage, and interpretation of the 49 GPR profiles was pursued using expertise, techniques, and tools borrowed from seismic reflection industry applications. The non-destructive GPR survey did not require special authorizations and was relatively fast and low cost. The pseudo-3D configuration

**Deleted:** But in cases like the VCT, GPR provided key parameters where no direct information on the nature of the surveyed deposits and no accurate dating is available, at the present day the GPR data assume a key-value

**Deleted:** currently

**Deleted:** event

**Deleted:** neither

**Deleted:** as well as

**Deleted:** the

**Deleted:** and

**Deleted:** ,

was an efficient compromise between spatial coverage and duration of the data acquisition (four days of fieldwork). On the other hand, the data processing was non-trivial, requiring about six months overall to set up an optimized workflow, due to challenging data characteristics, such as the steep and rugged topography and the sharp lateral variations of dielectrical properties of media (Triassic Dolostones vs Quaternary deposits). Our structural reconstruction derived by GPR data interpretation shows several sets of sub-vertical discontinuities within the near-surface (~ 1-4 m depth), which we interpreted as a pattern of extensional surface faulting. Such faults are bounding small local “graben or semi-graben-like” structures, which cut an hypothesized Holocene age clastic cover and underlying Triassic dolostones. We have also identified some chaotic and laterally discontinuous GPR-stratigraphic facies, interpreted as near-fault post-earthquake deposits (i.e. colluvial wedges ?). These shallow structures suggest the possibility that surface faulting due to past strong earthquakes ( $6 < M_w < 7$ ) occurred in relatively recent times in the study area. Its traces at surface were possibly later levelled by the concurrent natural processes of erosion, aggradation and, anthropogenic activities. As our results confirms the presence of seismic potential and thus the possible occurrence of a large earthquake in the future, we wish the primary effect of our study to be one of raising the level of attention regarding the seismic hazard in the Campotenese area, as well as prompting further research. Upon ground truthing, our work may represent a preparatory study for further geophysical surveys (3D GPR and other methods), as well as direct analysis including trenching, drilling, sampling campaigns and dating (e.g., luminescence, radiocarbon, etc). Although a further multidisciplinary approach would be necessary to achieve a quantitative (i.e. slip rates and recurrence times) assessment of the seismogenic potential of the study area, we firmly promote, particularly where near-surface data is lacking, a widespread use of the presented GPR workflow on other seismic gaps worldwide.

*Author contributions.* ME and DC contributed equally to this work as first authors. ME, DC, CP, FB led the fieldworks. ME analyzed, processed the GPR and GNSS data. ME, DC, CP, HMJ, FB contributed to the paper conceptualization and writing. ME and DC managed all data in the GIS environment and within 3D interpretation programs (OpendTect, Move), as well as they have created all the figures. DC realized the final 3D structural-geological model through Move software. All authors reviewed and edited all the drafts.

*Competing interests.* The authors declare that they have no conflict of interest.

*Disclaimer. Publisher's note:* Copernicus Publications remains neutral with regard to jurisdictional claims in published maps and institutional affiliations.

*Special issue statement.* This article is part of the special issue “Tools, data and models for 3-D seismotectonics: Italy as a key natural laboratory”.

## Acknowledgments

We sincerely thank Leonardo Speziali, Prof. Costanzo Federico, and Roberto Volpe for their support during the field operations, as well as Khayal Gavarof for his massive and valuable collaboration in data organization and processing. We thank QGIS (<https://www.qgis.org/it/site/>) for providing the software with an open-source license, Petroleum Experts (<https://www.petex.com/products/move-suite/>), and dGB (<https://www.dgbes.com/>) for providing the academic licenses MOVE and OpenDtect software. We acknowledge NETGEO for academic access to the NRTK network (<http://www.netgeo.it/>). We would also like to thank the Ministero dell'Ambiente e della Tutela del Territorio e del Mare (MATM) and the Regione Calabria for providing free access to geospatial data such as DTM and aerials (Regione Calabria - [www.regione.calabria.it](http://www.regione.calabria.it), under license IODL 2.0. - <https://www.dati.gov.it/iodl/2.0/>). We

**Deleted:** The study has benefited from several funding sources including: Agreement INGV-DPC 2012-2013 & 2014-2015, Project S1 – Miglioramento delle conoscenze per la definizione del potenziale sismogenetico - Base-knowledge improvement for assessing the seismogenic potential of Italy, <https://sites.google.com/site/ingvdpcprojects1/home>, resp. Cristina Pauselli, funded by Italian Presidenza del Consiglio dei Ministri – Dipartimento della Protezione Civile (DPC). The paper does not necessarily represent DPC official opinion and policy.



sincerely thank also the editor Luca de Siena and two anonymous reviewers for their constructive corrections and suggestions which contributed to improve our manuscript. The paper is the result of collaboration within the framework of the Interuniversity Center for 3D Seismotectonics with territorial applications - CRUST (<https://www.crust.unich.it/>). The GPR dataset presented in this study is available on request from the corresponding author.

---

*Financial support.* The study has benefited from several funding sources including: Agreement INGV-DPC 2012-2013 & 2014-2015, Project S1 – Miglioramento delle conoscenze per la definizione del potenziale sismogenetico - Base-knowledge improvement for assessing the seismogenic potential of Italy, <https://sites.google.com/site/ingvdpcprojects1/home>, resp. Cristina Pauselli, funded by Italian Presidenza del Consiglio dei Ministri – Dipartimento della Protezione Civile (DPC). The paper does not necessarily represent DPC official opinion and policy.

*Review statement.* This paper was edited by Luca De Siena and reviewed by two anonymous referee.

Formatted: Font: Italic

Formatted: Justified, Line spacing: 1.5 lines

## References

- Amicucci, L., Barchi, M.R., Montone, P., and Rubilani, N.: The Vallo di Diano and Auletta extensional basins in the southern Apennines (Italy): a simple model for a complex setting, *Terra Nova*, 20, 475-482, <https://doi.org/10.1111/j.1365-3121.2008.00841.x>, 2008.
- Amodio Morelli, L., Bonardi, G., Colonna, V., Dietrich, D., Giunta, G., Ippolito, F., Liguori, V., Lorenzoni, S., Paglionico, A., Perrone, V., Piccarreta, G., Russo, M., Scandone, P., Zanettin-Lorenzoni, E., and Zuppeta, A.: L'Arco calabro peloritano nell'orogene appenninico-maghrebide, *Mem. Soc. Geol. It.*, 17, 1-60, 1976.
- Anchuela, Ó.P., Lafuente, P., Arlegui, L., Liesa, C. L., and Simon, J. L.: Geophysical characterization of buried active faults: the Concud Fault (Iberian Chain, NE Spain), *Int J Earth Sci (Geol Rundsch)*, 105, 2221–2239, <https://doi.org/10.1007/s00531-015-1283-y>, 2016.
- Annan, A.P.: Ground-penetrating radar workshop notes, Sensors and Software Inc. Mississauga, ON, Canada, 192 pp., 2001.
- Ascione, A., Cinque, A., Santangelo, N., and Tozzi, M.: Il Bacino del Vallo di Diano e la tettonica trascorrente plio-quadernaria: nuovi vincoli cronologici e cinematici, *Stud. Geol. Camerti*, 1992/1, 201– 208, 1992a.
- Audru, J.C., Bano, M., Begg, J., Berryman, K., Henrys, S., and Niviere, B.: GPR investigations on active faults in urban areas: the Georisc-NZ project in Wellington, New Zealand, *Comptes Rendus de l'Academie des Sciences - Series IIA, Earth planet. Sci.*, 333(8), 447-454, [https://doi.org/10.1016/S1251-8050\(01\)01663-9](https://doi.org/10.1016/S1251-8050(01)01663-9), 2001.
- Bano, M., Edel, J.-B., Herquel G., and EPGS class 2001/2002: Geophysical investigation of a recent shallow fault, *The Leading Edge*, 21 (7), 648-650, <https://doi.org/10.1190/1.1497317>, 2002.
- Barchi, M.R., Lavecchia, G., Galadini, F., Messina P., Michetti, A. M., Peruzza, L., Pizzi, A., Tondi, E., and Vittori, E.: Sintesi delle conoscenze sulle faglie attive in Italia Centrale: parametrizzazione ai fini della caratterizzazione della pericolosità sismica, CNR-GNDT, Projects 5.1.2, 6a2, 5.1.1, Esagrafica, Roma, 2000.
- Barchi, M.R., Carboni, F., Michele, M., Ercoli, M., Giorgetti, C., Porreca, M., Azzaro, S., Chiaraluce, L.: The influence of subsurface geology on the distribution of earthquakes during the 2016–2017 Central Italy seismic sequence, *Tectonophysics*, 807, 228797, <https://doi.org/10.1016/j.tecto.2021.228797>, 2021.
- Bello S., de Nardis R., Scarpa R., Brozzetti F., Cirillo D., Ferrarini F., di Lieto B., Arrowsmith R. J., Lavecchia G.: Fault Pattern and Seismotectonic Style of the Campania – Lucania 1980 Earthquake (Mw 6.9, Southern Italy): New Multidisciplinary Constraints”, *Frontiers in Earth Science*, 8, 652, <https://doi.org/10.3389/feart.2020.608063>, 2021.
- Benson, A.K.: Applications of ground penetrating radar in assessing some geological hazards: examples of groundwater contamination, faults, cavities, *Journal of Applied Geophysics*, 33(1–3), 177–193, [https://doi.org/10.1016/0926-9851\(95\)90040-3](https://doi.org/10.1016/0926-9851(95)90040-3), 1995.
- Beres, M., Huggenberger, P., Green, A. G., and Horstmeyer, H.: Using two- and three-dimensional georadar methods to characterize glaciofluvial architecture, *Sediment. Geol.*, 129, 1-24, 1999.
- Boncio, P., Pizzi, A., Brozzetti, F., Pomposo, G., Lavecchia, G., Di Naccio, D., and Ferrarini, F., Coseismic ground deformation of the 6 april 2009 L'Aquila earthquake (central Italy, Mw 6.3), *Geoph. Res. Lett.*, 37, <http://dx.doi.org/10.1029/2010GL042807>, 2010.
- Brandes, C., Igel, J., Loewer, M., Tanner, D., C., Lang, J., Müller, K., and Winseman, J.: Visualisation and analysis of shear-deformation bands in unconsolidated Pleistocene sand using ground-penetrating radar: Implications for paleoseismological studies, *Sedimentary Geology*, 367, 135-145, <https://doi.org/10.1016/j.sedgeo.2018.02.005>, 2018.

1 Bricheva, S.S., Dubrovin, I.O., Lunina, O.V., Denisenko, I.A., Matasov, V.M., Turova, I.V., Entin, A.L., Panin, A.V.,  
2 and Deev, E.V.: Numerical simulation of ground-penetrating radar data for studying the geometry of fault zone, Near  
3 Surface Geophysics, Accepted Author Manuscript, <https://doi.org/10.1002/nsg.12153>, 2021.

4 Bristow, C.S., and Jol, H.M.: GPR in sediments: advice on data collection, basic processing and interpretation, a good  
5 practice guide, In: Ground Penetrating Radar in Sediments, (Eds C.S. Bristow and H.M. Jol) Geol. Soc. Spec. Publ.,  
6 211, 1-7, <https://doi.org/10.1144/GSL.SP.2001.211.01.02>, 2003.

7 Brozzetti, F., and Lavecchia, G.: Seismicity and related extensional stress field: the case of the Norcia Seismic Zone  
8 (Central Italy), *Ann. Tectonicae*, 8(1), 36–57, 1994.

9 Brozzetti, F., Lavecchia, G., Mancini, G., Milana G., and Cardinali, M.: Analysis of the 9 September 1998 Mw 5.6  
10 Mercure earthquake sequence (southern Apennines, Italy): a multidisciplinary approach, *Tectonophysics*, 476, 210–  
11 225, <https://doi.org/10.1016/j.tecto.2008.12.007>, 2009.

12 Brozzetti, F.: The Campania-Lucania extensional fault system (southern Italy): a suggestion for a uniform model of  
13 active extension in the Italian Apennines, *Tectonics*, 30 (5), 1-26, TC5009, <http://dx.doi.org/10.1029/2010TC002794>,  
14 2011.

15 Brozzetti, F., Cirillo, D., de Nardis, R., Lavecchia, G., and Cardinali, M.: Detailed mapping of active faults in the  
16 Calabro-Lucania Region, Report INGV-DPC 2014-2015 project S1 "Base-knowledge improvement for assessing the  
17 seismogenic potential of Italy, <https://sites.google.com/site/ingvdp/projects1/home>, 2015.

18 Brozzetti, F., Cirillo, D., de Nardis, R., Cardinali, M., Lavecchia, G., Orecchio, B., Presti D., and Totaro, C.: Newly  
19 identified active faults in the Pollino seismic gap, southern Italy, and their seismotectonic significance, *J. Struct. Geol.*,  
20 94, 13-31, <https://doi.org/10.1016/j.jsg.2016.10.005>, 2017a.

21 Brozzetti, F., Cirillo, D., Liberi, F., Piluso, E., Faraca, E., De Nardis, R., and Lavecchia, G.: Structural style of  
22 Quaternary extension in the Crati Valley (Calabrian Arc): Evidence in support of an east-dipping detachment fault, *It.*  
23 *Journ. of Geosci.*, 136(3), 434-453, <https://doi.org/10.3301/IJG.2017.11>, 2017b.

24 Brozzetti, F., Boncio, P., Cirillo, D., Ferrarini, F., de Nardis, R., Testa, A., Liberi, F., and Lavecchia, G.: High  
25 resolution field mapping and analysis of the August–October 2016 coseismic surface faulting (Central Italy  
26 Earthquakes): slip distribution, parameterization and comparison with global earthquakes, *Tectonics*, 38, 417–439,  
27 <https://doi.org/10.1029/2018TC005305>, 2019.

28 Brozzetti, F., Mondini, A.C., Pauselli, C., Mancinelli, P., Cirillo, D., Guzzetti, F., and Lavecchia, G.: Mainshock  
29 anticipated by intra-sequence ground deformations: Insights from multiscale field and SAR interferometric  
30 measurements, *Geosciences (Switzerland)*, 10(5), 186, <https://doi.org/10.3390/geosciences10050186>, 2020.

31 Bubeck, A., Wilkinson, M., Roberts, G.P., Cowie, P. A., McCaffrey, K.J.W., Phillips, R., and Sammonds, P.: The  
32 tectonic geomorphology of bedrock scarps on active normal faults in the Italian Apennines mapped using combined  
33 ground penetrating radar and terrestrial laser scanning, *Geomorphology*, 237, 38-51,  
34 <https://doi.org/10.1016/j.geomorph.2014.03.011>, 2015.

35 Busby, J.P., and Merritt, J.W.: Quaternary deformation mapping with ground penetrating radar, *J. appl. Geophys.*,  
36 41(1), 75–91, [https://doi.org/10.1016/S0926-9851\(98\)00050-.0](https://doi.org/10.1016/S0926-9851(98)00050-.0), 1999.

37 Cai, J., McMechan, G.A., and Fisher, M.A.: Application of ground penetrating radar to investigation of near-surface  
38 fault properties in the San Francisco Bay region, *Bull. seism. Soc. Am.*, 86(5), 1459-1470, Available online: (accessed  
39 09 feb 2021), <https://citeseerx.ist.psu.edu/viewdoc/download?doi=10.1.1.944.4417&rep=rep1&type=pdf>, 1996.

1 Calamita, F., Pizzi, A., and Roscioni, M.: I fasci di faglie recenti ed attive di M. Vettore - M. Bove e di M. Castello -  
2 M. Cardosa (Appennino Umbro-Marchigiano), In *Studi Geologici Camerti*; Università di Camerino: Camerino, Italy,  
3 1992; 81-95, Available online: <http://193.204.8.201:8080/jspui/handle/1336/552> (accessed on 09 Feb 2021), 1992.

4 Carpentier, S.F.A., Green, A.G., Langridge, R., Boschetti, S., Doetsch, J., Abacherli, A.N., Horstmeyer, H., and  
5 Finnemore, M.: Flower structures and Riedel shears at a step over zone along the Alpine Fault (New Zealand) inferred  
6 from 2-D and 3-D GPR images, *Journal Geophysical Research*, 117(B2), B02406,  
7 <https://doi.org/10.1029/2011JB008749>, 2012a.

8 Carpentier, S.F.A., Green, A.G., Doetsch, J., Dorn, C., Kaiser, A.E., Campbell, F., Horstmeyer, H., and Finnemore,  
9 M.: Recent deformation of Quaternary sediments as inferred from GPR images and shallow P-wave velocity  
10 tomograms: Northwest Canterbury Plains, New Zealand, *J. Appl. Geophys.*, 8, 2-15,  
11 <https://doi.org/10.1016/j.jappgeo.2011.09.007>, 2012b.

12 Cello G., E. Tondi, L. Micarelli, and L. Mattioni: Active tectonics and earthquake sources in the epicentral area of the  
13 1857 Basilicata earthquake (southern Italy), *Journal of Geodynamics*, 36, 1–2, 37-50, [https://doi.org/10.1016/S0264-](https://doi.org/10.1016/S0264-3707(03)00037-1)  
14 [3707\(03\)00037-1](https://doi.org/10.1016/S0264-3707(03)00037-1), 2003.

15 Chiaraluce, L., Di Stefano, R., Tinti, E., Scognamiglio, L., Michele, M., Casarotti, E., Cattaneo, M., De Gori, P.,  
16 Chiarabba, C., Monachesi, G., Lombardi, A., Valoroso, L., Latorre, D., and Marzorati, S.: The 2016 Central Italy  
17 Seismic Sequence: A First Look at the Mainshocks, Aftershocks, and Source Models, *Seismological Research Letters*,  
18 88(3), 757-771, <https://doi.org/10.1785/0220160221>, 2017.

19 Christie, M., Tsoflas, G.P., Stockli, D.F., and Black, R.: Assessing fault displacement and off-fault deformation in an  
20 extensional tectonic setting using 3-D ground-penetrating radar imaging, *J. appl. Geophys.*, 68(1), 9–16,  
21 <https://doi.org/10.1016/j.jappgeo.2008.10.013>, 2009.

22 Cinti, F. R., Cucci, L., Pantosti, D., D'Addezio, G., and Meghraoui, M.: A major seismogenic fault in a 'silent area':  
23 the Castrovillari fault (southern Apennines, Italy), *Geophysical Journal International*, 130(3), 595-605, Available  
24 online: (accessed 09 Feb 2021), <https://www.earth-prints.org/bitstream/2122/12031/1/text.pdf>, 1997.

25 Cinti, F. R., Moro, M., Pantosti, D., Cucci, L., and D'Addezio, G.: New constraints on the seismic history of the  
26 Castrovillari fault in the Pollino gap (Calabria, southern Italy), *J. Seismol.*, 6, 199-217,  
27 <https://doi.org/10.1023/A:1015693127008>, 2002.

28 Cinti, F.R., Pauselli, C., Livio, F., Ercoli, M., Brunori, C.A., Ferrario, F., Volpe, R., Civico, R., Pantosti, D., Pinzi, S.,  
29 De Martini, P.M., Ventura, G., Alfonsi, L., Gambillara, R., and Michetti, A.M.: Integrating multidisciplinary, multi-  
30 scale geological and geophysical data to image the Castrovillari fault (Northern Calabria, Italy), *Geophys. J. Int.*, 203,  
31 1847-1863, <https://doi.org/10.1093/gji/ggv404>, 2015a.

32 Cinti, F.R., L. Alfonsi, A. D'Alessio, S. Marino, C.A. Brunori: Faulting and Ancient Earthquakes at Sybaris  
33 archaeological site, Ionian Calabria, Southern Italy, *Seism. Res. Lett.*, 86, 1, doi: 10.1785/02201401071, 2015b.

34 Cinti, F. R., De Martini, P. M., Pantosti, D., Baize, S., Smedile, A., Villani, F., et al.: 22-kyr-long record of surface  
35 faulting along the source of the 30 October 2016 earthquake (central Apennines, Italy), from integrated paleoseismic  
36 data sets. *Journal of Geophysical Research: Solid Earth*, 124, <https://doi.org/10.1029/2019JB017757>, 2019.

37 Cirillo, D., Totaro, C., Lavecchia, G., Orecchio, B., de Nardis, R., Presti, D., Ferrarini, F., Bello, S., and Brozzetti, F.:  
38 Structural complexities and tectonic barriers controlling recent seismic activity of the Pollino area (Calabria-Lucania,  
39 Southern Italy) – constraints from stress inversion and 3D fault model building, *Solid Earth Discuss.* [preprint],  
40 <https://doi.org/10.5194/se-2021-76>, in review, 2021.

1 Cirillo, D.: Digital Field Mapping and Drone-Aided Survey for Structural Geological Data Collection and Seismic  
2 Hazard Assessment: Case of the 2016 Central Italy Earthquakes, *Applied Sciences*, 10,  
3 5233, <https://doi.org/10.3390/app10155233>, 2020.

4 Conyers, L.B.: *Ground-penetrating Radar for Geoarchaeology*, Wiley-Blackwell, London, Wiley Online Library, 160  
5 pp., doi:10.1002/9781118949993, 2016.

6 Daniels, D. J., *Ground Penetrating Radar. Radar, Sonar and amp; Navigation*, Institution of Engineering and  
7 Technology, London: IEE Press, 752 pp, <https://doi.org/10.1002/0471654507.emc152>, 2004.

8 Davis, J.L., and Annan, A.P.: Ground penetrating radar for high resolution mapping of soil and rock stratigraphy,  
9 *Geophys. Prospect.*, 37, 531-551, 1989.

10 Demanet, F., Renardy, D., Vanneste, K., Jongmans, D., Camelbeeck, T., and Meghraoui, M.: The use of geophysical  
11 prospecting for imaging active faults in the Roer Graben, Belgium, *Geophysics*, 66(1), 78–89,  
12 <https://doi.org/10.1190/1.1444925>, 2001.

13 Dujardin, J. R., and Bano, M.: Topographic migration of GPR data: Examples from Chad and Mongolia, *Comptes*  
14 *Rendus Geoscience*, 345, 2, 73-80, <https://doi.org/10.1016/j.crte.2013.01.003>, 2013.

15 Ercoli, M., Pauselli, C., Frigeri, A., Forte, E., and Federico, C.: “Geophysical paleoseismology” through high  
16 resolution GPR data: A case of shallow faulting imaging in Central Italy, *Journal of Applied Geophysics*, 90, 27-40,  
17 <https://doi.org/10.1016/j.jappgeo.2012.12.001>, 2013a.

18 Ercoli, M., Pauselli, C., Forte, E., Frigeri, A., and Federico, C.: The Mt. Pollino Fault (southern Apennines, Italy):  
19 GPR signature of Holocene earthquakes in “silent” area, in: 7th Int. Work. Adv. Gr. Penetrating Radar, IEEE, 1–6,  
20 <https://doi.org/10.1109/IWAGPR.2013.6601510>, 2013b.

21 Ercoli, M., Pauselli, C., Frigeri, A., Forte, E., and Federico, C.: 3-D GPR data analysis for high-resolution imaging of  
22 shallow subsurface faults: The Mt Vettore case study (Central Apennines, Italy), *Geoph. J. Int.*, 198(1), 609-621,  
23 <https://doi.org/10.1093/gji/ggu156>, 2014.

24 Ercoli, M., Pauselli, C., Cinti, F.R., Forte, E., and Volpe, R.: Imaging of an active fault: Comparison between 3D GPR  
25 data and outcrops at the Castrovillari fault, Calabria, Italy, *Interpretation*, 3(3), SY57-SY66,  
26 <https://doi.org/10.1190/INT-2014-0234.1>, 2015.

27 Ercoli, M., Di Matteo, L., Pauselli, C., Mancinelli, P., Frapiccini, S., Talegalli, L., and Cannata, A.: Integrated GPR  
28 and laboratory water content measures of sandy soils: From laboratory to field scale, *Construction and Building*  
29 *Materials*, 159,734-744, <https://doi.org/10.1016/j.conbuildmat.2017.11.082>, 2018.

30 Ercoli, M., Forte, E., Porreca, M., Carbonell, R., Pauselli, C., Minelli, G., and Barchi, M. R.: Using seismic attributes  
31 in seismotectonic research: an application to the Norcia Mw = 6.5 earthquake (30 October 2016) in central Italy, *Solid*  
32 *Earth*, 11, 329-348, <https://doi.org/10.5194/se-11-329-2020>, 2020.

33 Ferrarini, F., de Nardis, R., Brozzetti, F., Cirillo, D., Arrowsmith, J. R. and Lavecchia, G.: Multiple Lines of Evidence  
34 for a Potentially Seismogenic Fault Along the Central-Apennine (Italy) Active Extensional Belt—An Unexpected  
35 Outcome of the MW6.5 Norcia 2016 Earthquake, *Front. Earth Sci.*, 9:642243, doi: 10.3389/feart.2021.642243, 2021.

36 Ferrario, M. F., & Livio, F., Characterizing the distributed faulting during the 30 October 2016, Central Italy  
37 earthquake: A reference for fault displacement hazard assessment, *Tectonics*, 37,  
38 <https://doi.org/10.1029/2017TC004935>, 2018.

39 Filice, F., Liberi, F., Cirillo, D., Pandolfi, L., Marroni, M., and Piluso E.: Geology map of the central area of Catena  
40 Costiera: insights into the tectono-metamorphic evolution of the Alpine belt in Northern Calabria, *Journal of Maps*,  
41 11(1), 114-125, <https://doi.org/10.1080/17445647.2014.944877>, 2015.

**Deleted:** Cirillo, D., Totaro, C., Lavecchia, G., Orecchio, B., de Nardis, R., Presti, D., Ferrarini, F., Bello, S., and Brozzetti, F.: Structural complexities and tectonic barriers controlling recent seismic activity of the Pollino area (Calabria-Lucania, Southern Italy) – constraints from stress inversion and 3D fault model building, preprint of this special issue, *Solid Earth*, <https://doi.org/10.5194/se-2021-76>, 2021.¶

1 Filice, F., and Seeber, L.: The Culmination of an Oblique Time-Transgressive Arc Continent Collision: The Pollino  
2 Massif Between Calabria and the Southern Apennines, Italy, *Tectonics*, 38(1), 3261-3280,  
3 <https://doi.org/10.1029/2017TC004932>, 2019.

4 Forte, E., and Pipan, M.: Review of multi-offset GPR applications: Data acquisition, processing and analysis, *Signal*  
5 *Processing*, 132, 210-220, <https://doi.org/10.1016/j.sigpro.2016.04.011>, 2017.

6 Frigeri, A., and Ercoli, M.: The ScanMars Subsurface Radar Sounding Experiment on AMADEE-18, *Astrobiology*,  
7 20(11), 1338-1352, <https://doi.org/10.1089/ast.2019.2037>, 2020.

8 Gafarov, K., Ercoli, M., Cirillo, D., Pauselli, C., and Brozzetti, F.: Extending surface geology data through GPR  
9 prospectons: Quaternary faulting signature from the Campotenese area (Calabria-Italy), 2018 17th International  
10 Conference on Ground Penetrating Radar (GPR), Rapperswil, pp. 1-4, doi: 10.1109/ICGPR.2018.8441611, 2018.

11 Galadini, F., C. Meletti, and E. Vittori: Major active faults in Italy: Available surficial data, *Netherlands J. Geosci.*  
12 80, nos. 3/4, 273-296, 2001.

13 Galadini, F., and Galli, P.: Paleoseismology of silent faults in the Central Apennines (Italy): the Mt. Vettore and Laga  
14 Mts. Faults, *Annals of Geophysics*, 46(5), 815-836, <https://doi.org/10.4401/ag-3457>, 2003.

15 Galli, P., Galderisi, A., Peronace, E., Giaccio, B., Hajdas, I., Messina, P., Pileggi, D., and Polpetta, F.: The awakening  
16 of the dormant Mount Vettore fault (2016 central Italy earthquake, Mw 6.6): Paleoseismic clues on its millennial  
17 silences, *Tectonics*, 38, 687-705, <https://doi.org/10.1029/2018TC005326>, 2019.

18 Galli, P.: Recurrence times of central-southern Apennine faults (Italy): Hints from paleoseismology, *Terra Nova*, 32,  
19 399-407, <https://doi.org/10.1111/ter.12470>, 2020.

20 Geoportale Nazionale – Lidar data 1 m resolution, Ministero dell’Ambiente e della Tutela del Territorio e del Mare –  
21 Creative Commons License (Cc BY-SA 3.0 IT), last access February 2018.

22 Ghisetti, F., and Vezzani, L.: Structural Map of Mt. Pollino (Southern Italy), 1:50.000 Scale, SELCA, Firenze, 1983.

23 Goodman, D., Hongo, H., Higashi, N., Inaoka, H., and Nishimura, Y.: GPR surveying over burial mounds: correcting  
24 for topography and the tilt of the GPR antenna, *Near Surface Geophysics*, 5, 383-388, [https://doi.org/10.3997/1873-](https://doi.org/10.3997/1873-0604.2007020)  
25 [0604.2007020](https://doi.org/10.3997/1873-0604.2007020), 2007.

26 Goodman, D., and Piro S.: GPR Remote Sensing in Archaeology Springer Science & Business Media (ISBN: 978–3-  
27 642-31856-6), doi: 10.1007/978-3-642-31857-3, 2013.

28 Grandjaquet, C.L., and Grandjaquet, M.J.: Geologie de la zone de Diamante-Verbicaro (Calabre), *Geol. Romana* 1,  
29 297-312, Available online: (accessed 09 Feb 2021), <http://www.dst.uniroma1.it/VolumeI>, 1962.

30 Grasmueck, M.: 3-D ground-penetrating radar applied to fracture imaging in gneiss, *Geophysics*, 61(4), 1050-1064,  
31 <https://doi.org/10.1190/1.1444026>, 1996.

32 Grasmueck, M., Weger, R., and Horstmeyer, H.: Full-resolution 3D GPR imaging, *Geophysics*, 70(1), K12-K19,  
33 2005.

34 Green, A.G., Gross, R., Holliger, K., Horstmeyer, H., and Baldwin, J.: Results of 3-D georadar surveying and  
35 trenching the San Andreas fault near its northern landward limit, *Tectonophysics*, 368, 7-23,  
36 [https://doi.org/10.1016/S0040-1951\(03\)00147-1](https://doi.org/10.1016/S0040-1951(03)00147-1), 2003.

37 Gross, R., Green, A.G., Holliger, K., Horstmeyer, H., and Baldwin, J.: Shallow geometry and displacements on the  
38 San Andreas Fault near Point Arena based on trenching and 3-D georadar surveying, *Geophysical Research Letters*,  
39 29(20), 34-1-34-4, <https://doi.org/10.1029/2002GL015534>, 2002.

1 Gross, R., Green, A.G., Horstmeyer, H., Holliger, K., and Baldwin, J.: 3-D georadar images of an active fault: efficient  
2 data acquisition, processing and interpretation strategies, *Subsurf. Sens. Technol. Appl.*, 4(1), 19-40,  
3 <https://doi.org/10.1023/A:1023059329899>, 2003.

4 Gross, R., Green, A.G., Horstmeyer, H., and Begg, J.H.: Location and geometry of the Wellington Fault (New  
5 Zealand) defined by detailed three-dimensional georadar data, *J. geophys. Res.*, 109, B05401,  
6 <https://doi.org/10.1029/2003JB002615>, 2004.

7 Heincke, B., Green, A.G., van der Kruk, J., and Willenberg, H.: Semblance-based topographic migration (SBTM): A  
8 method for identifying fracture zones in 3D georadar data, *Near Surface Geophysics*, 4(2), 79-88,  
9 <https://doi.org/10.3997/1873-0604.2005034>, 2006.

10 Huggenberger, P.: Radar facies: recognition of facies patterns and heterogeneities within Pleistocene Rhine gravels,  
11 NE Switzerland, In *Braided Rivers*, edited by J.L. Best and C.S. Bristow, *Geol. Soc. London Spec. Publ.*, 75, 163-  
12 176, 1993.

13 Istituto Nazionale di Geofisica e Vulcanologia - INGV (2020 February, last access), <https://data.ingv.it/en/>.

14 Iannace, A., D'Errico, M., and Vitale, S.: Carta Geologica dell'area compresa tra Maratea, Castrovillari e Sangineto,  
15 In: Vitale, S., Iannace, A. (Eds.), *Analisi Dello Strain Finito in 3D Dell'Unità Pollino-Ciagola (Confine Calabro-*  
16 *lucano, Italia Meridionale)*, Studi Geologici Camerti, Nuova Serie, 2, 153-167 (ISSN: 0392-0631), 2004.

17 Iannace, A., Garcia Tortosa, F.J., and Vitale, S.: The Triassic metasedimentary successions across the boundary  
18 between Southern Apennines and Calabria-Peloritani Arc (Northern Calabria, Italy), *Geol. J.*, 40, 155-171,  
19 <https://doi.org/10.1002/gj.1001>, 2005.

20 Iannace, A., Vitale, S., D'Errico, M., Mazzoli, S., Di Staso, A., Macaione, E., Messina, A., Reddy, S.M., Somma, R.,  
21 Zamparelli, V., Zattin, M., and Bonardi, G.: The carbonate tectonic units of northern Calabria (Italy): a record of  
22 Apulian palaeomargin evolution and Miocene convergence, continental crust subduction, and exhumation of HP-LT  
23 rocks, *J. Geol. Soc. Lond.*, 164, 1165-1186, <https://doi.org/10.1144/0016-76492007-017>, 2007.

24 Imposa, S., De Guidi, G., Grassi, S., Scudero, S., Barreca, G., Patti, G., and Boso, D.: Applying geophysical techniques  
25 to investigate a segment of a creeping fault in the urban area of San Gregorio di Catania, southern flank of Mt. Etna  
26 (Sicily - Italy), *Journal of Applied Geophysics*, 123, 153-163, <https://doi.org/10.1016/j.jappgeo.2015.10.008>, 2015.

27 ISIDe Working Group, Italian Seismological Instrumental and Parametric Database (ISIDe), Istituto Nazionale di  
28 Geofisica e Vulcanologia (INGV), <https://doi.org/10.13127/ISIDE>, 2007.

29 Jewell, C.J., and Bristow, C.S.: GPR studies in the Piano di Pezza area of the Ovindoli-Pezza Fault, Central Apennines,  
30 Italy: Extending palaeoseismic trench investigations with high resolution GPR profiling, *Near Surface Geophysics*,  
31 4(3), 147-153, <https://doi.org/10.3997/1873-0604.2005040>, 2006.

32 Jol, H.M.: *Ground Penetrating Radar: Theory and Applications*, Elsevier, pp 544, ISBN: 9780444533487, 2009.

33 Lehmann, F., and Green, A.G.: Topographic migration of georadar data: Implications for acquisition and processing,  
34 *Geophysics*, 65(3), 836-848, <https://doi.org/10.1190/1.1444781>, 2000.

35 Leonard, M.: Earthquake fault scaling: Relating rupture length, width, average displacement, and moment release,  
36 *Bull. Seismol. Soc. Am.*, 100(5A), 1971-1988, <https://doi.org/10.1785/0120090189>, 2010.

37 Liberi, F., Morten, L., and Piluso, E.: Geodynamic significance of the ophiolites within the Calabrian Arc. *Island Arc*,  
38 15, 26-43, <https://doi.org/10.1111/j.1440-1738.2006.00520.x>, 2006.

39 Liberty, L.M., Hemphill-Haley, M.A., and Madin, I.P.: The Portland Hills Fault: uncovering a hidden fault in Portland,  
40 Oregon using high resolution geophysical methods, *Tectonophysics*, 368(1-4), 89-103, [https://doi.org/10.1016/S0040-](https://doi.org/10.1016/S0040-1951(03)00152-5)  
41 [1951\(03\)00152-5](https://doi.org/10.1016/S0040-1951(03)00152-5), 2003.

1 Liner, C.L., and Liner, J.L.: Application of GPR to a site investigation involving shallow faults, *The Leading Edge*,  
2 16(11), 1649-1651, <https://doi.org/10.1190/1.1437545>, 1997.

3 Malik, J.N., Sahoo, A.K., and Shah, A.A.: Ground-penetrating radar investigation along Pinjore Garden Fault:  
4 implication toward identification of shallow subsurface deformation along active fault, NW Himalaya, *Curr. Sci.*,  
5 93(10), 1422-1427, 2007.

6 Malik, J. N., Kumar, A., Satuluri, S., Puhan, B., and Mohanty, A.: Ground-Penetrating Radar Investigations along  
7 Hajipur Fault: Himalayan Frontal Thrust-Attempt to Identify Near Subsurface Displacement, NW Himalaya, India",  
8 *International Journal of Geophysics*, Article ID 608269, 7 pp., <https://doi.org/10.1155/2012/608269>, 2012.

9 Maschio, L., Ferranti, L., and Burrato, P.: Active extension in Val d'Agri area, southern Apennines, Italy: Implications  
10 for the geometry of the seismogenic belt, *Geophys. J. Int.*, 162, 591–609, [https://doi.org/10.1111/j.1365-](https://doi.org/10.1111/j.1365-246X.2005.02597.x)  
11 [246X.2005.02597.x](https://doi.org/10.1111/j.1365-246X.2005.02597.x), 2005.

12 Matoš, B., Zajc, M., Kordić, B., Tomljenović, B., and Gosar, A.: Quaternary fault activity in the SW Pannonian Basin:  
13 GPR surveying in the Bilogora Mt. (NE Croatia), *Geological Quarterly*, 61(1), 18–36, doi:  
14 <https://doi.org/10.7306/gq.1308>, 2017.

15 McCalpin, J.P.: *Paleoseismology*, 2nd Edition, International Geophysics Series, 95, Elsevier Publishing, 647 pp., plus  
16 additional website content at: [www.elsevier.com](http://www.elsevier.com), ISBN 978-0-12-373576-8, 2009.

17 McCann, W.R., Nishenko, S.P., Sykes, I.R., and Krause, J.: Seismic gaps and plate tectonics: seismic potential for  
18 major boundaries, *Pure and applied geophysics*, 117, 1082–1147, 1979.

19 McClymont, A.F., Green, A.G., Villamor, P., Horstmeyer, H., Grass, C., and Nobes, D.C.: Characterization of the  
20 shallow structures of active fault zones using 3-D GPR data, *J. geophys. Res.*, 113, B10315,  
21 <https://doi.org/10.1029/2007JB005402>, 2008.

22 McClymont, A.F., Villamor, P., and Green, A.G.: Fault displacement accumulation and slip rate variability within the  
23 Taupo Rift (New Zealand) based on trench and 3-D ground-penetrating radar data, *Tectonics*, 28, TC4005,  
24 <https://doi.org/10.1029/2008TC002334>, 2009.

25 McClymont, A.F., Green, A.G., Kaiser, A., Horstmeyer, H., and Langridge, R.: Shallow fault segmentation of the  
26 Alpine fault zone, New Zealand revealed from 2- and 3-D GPR surveying, *J. Appl. Geophys.*, 70(4), 343–354,  
27 <https://doi.org/10.1016/j.jappgeo.2009.08.003>, 2010.

28 Michele, M., Chiaraluce, L., Di Stefano, R., & Waldhauser, F.: Fine-scale structure of the 2016–2017 Central Italy  
29 seismic sequence from data recorded at the Italian National Network. *Journal of Geophysical Research: Solid Earth*,  
30 125, e2019JB018440, <https://doi.org/10.1029/2019JB018440>, 2020.

31 Michetti, A. M., Ferrelì, L., Serva, L., and Vittori, E.: Geological evidence for strong historical earthquakes in an  
32 "aseismic" region: The Pollino case (Southern Italy), *Journal of Geodynamics*, 24:1–4, 67–86,  
33 [https://doi.org/10.1016/S0264-3707\(97\)00018-5](https://doi.org/10.1016/S0264-3707(97)00018-5), 1997.

34 Michetti, A. M., Ferrelì, L., Esposito, E., Porfido, S., Blumetti, A. M., Vittori, E., Serva, L., and Roberts, G. P.: Ground  
35 Effects during the 9 September 1998, Mw = 5.6 Lauria, Earthquake and the Seismic Potential of the seismic Pollino  
36 Region in Southern Italy, *Seismological Research Letters*, 71(1), 31–46, <https://doi.org/10.1785/gssrl.71.1.31>, 2000.

37 Mogi K.: Two Kinds of Seismic Gaps. In: Wyss M. (eds) *Earthquake Prediction and Seismicity Patterns*, Contributions  
38 to Current Research in Geophysics, Birkhäuser, Basel, [https://doi.org/10.1007/978-3-0348-6430-5\\_4](https://doi.org/10.1007/978-3-0348-6430-5_4), 1979.

39 Napolitano, F., De Siena, L., Gervasi, A., Guerra, I., Scarpa, R., and La Rocca, M.: Scattering and absorption imaging  
40 of a highly fractured fluid-filled seismogenic volume in a region of slow deformation, *Geosci. Front.*, 11(3), 989–  
41 998, <https://doi.org/10.1016/j.gsf.2019.09.014>, 2020.



1 Napolitano, F., Galluzzo, D., Gervasi, A., Scarpa, R., and La Rocca, M.: Fault imaging at Mt Pollino (Italy) from  
2 relative location of microearthquakes, *Geophysical Journal International*, 224(1), 637-  
3 648, <https://doi.org/10.1093/gji/ggaa407>, 2021.

4 Nobes, D. C., Jol, H. M., and Duffy, B.: Geophysical imaging of disrupted coastal dune stratigraphy and possible  
5 mechanisms, Haast, South Westland, New Zealand, *New Zealand Journal of Geology and Geophysics*, 59:3, 426-435,  
6 doi: 10.1080/00288306.2016.1168455, 2016.

7 Oddone, E.: Gli elementi fisici del grande terremoto marsicano-fucense del 13 gennaio 1915. *Boll. Soc. Sismol. Ital.*  
8 19, 71-216, 1915

9 Ogniben, L.: Schema introduttivo alla geologia del confine calabro-lucano, *Mem. Soc. Geol. It.* 8, 453-763, 1969.

10 Overgaard, T. and Jakobsen, P.R.: Mapping of glaciotectionic deformation in an ice marginal environment with ground  
11 penetrating radar, *Journal Applied Geophysics*, 47(3-4), 191-197, [https://doi.org/10.1016/S0926-9851\(01\)00064-7](https://doi.org/10.1016/S0926-9851(01)00064-7),  
12 2001.

13 Passarelli, L., Hainzl, S., Cesca, S., Maccaferri, F., Mucciarelli, M., Roessler, D., Corbi, F., Dahm, T., Rivalta, E.:  
14 Aseismic transient driving the swarm-like seismic sequence in the Pollino range, Southern Italy, *Geophysical Journal*  
15 *International*, 201:3, 1553–1567, <https://doi.org/10.1093/gji/ggv111>, 2015.

16 Pantosti, D. and Valensise, G.: Faulting mechanism and complexity of the November 23, 1980, Campania-Lucania  
17 earthquake, inferred from surface observations, *J. Geophys. Res.*, 95(B10), 15,319-15,341,  
18 <https://doi.org/10.1029/JB095iB10p15319>, 1990.

19 Pastori, M., Margheriti, L., De Gori, P., Govoni, A., Lucente, F.P., Moretti, M., Marchetti, A., Di Giovambattista, R.,  
20 Anselmi, M., De Luca, P., Nardi, A., Agostinetti, N.P., Latorre, D., Piccinini, D., Passarelli, L., and Chiarabba, C.:  
21 The 2011–2014 Pollino Seismic Swarm: Complex Fault Systems Imaged by 1D Refined Location and Shear Wave  
22 Splitting Analysis at the Apennines–Calabrian Arc Boundary, *Front. Earth Sci.*, 9:618293, doi:  
23 10.3389/feart.2021.618293, 2021.

24 Patacca, E. and Scandone, P.: Geological interpretation of the CROP-04 seismic line (Southern Apennines, Italy),  
25 *Boll. Soc. Geol. It. (Ital. J. Geosci.)*, 7, 297-315, 2007.

26 Pauselli, C., Federico, C., Frigeri, A., Orosei, R., Barchi, M.R., and Basile, G.: Ground Penetrating Radar  
27 investigations to study active faults in the Norcia Basin (Central Italy), *J. Appl. Geophys.*, 72, 39-45,  
28 <https://doi.org/10.1016/j.jappgeo.2010.06.009>, 2010.

29 Pauselli, C., Ercoli, M. Volpe, R. Federico, C. Mazzocca, M., and Speziali, L.: 2D and 3D GPR images of selected  
30 fault planes (Calabro-Lucania border), Report DPC-INGV-S1 Project "Base-knowledge improvement for assessing  
31 the seismogenic potential of Italy", deliverable D18/c1.1 - (<https://sites.google.com/site/ingvdpctrprojects1/documents>,  
32 Agreement INGV-DPC 2014-2015), 49 pp., 2015.

33 Plafker, G. and Galloway, J. P.: Lessons Learned from the Lorna Prieta, California, Earthquake of October 17, 1989,  
34 *USGS Numbered Series Circular* 1045, 48 pp., <https://doi.org/10.3133/cir1045>, 1989.

35 Pondrelli, S., Salimbeni, S., Ekström, G., Morelli, A., Gasperini, P., and Vannucci, P.: The Italian CMT dataset from  
36 1977 to present, *Phys. Earth Plan. Int.*, 159, 286-303, 2006.

37 Porreca, M., Minelli, G., Ercoli, M., Brobia, A., Mancinelli, P., Cruciani, F., Giorgetti, C., Carboni, F., Mirabella, F.,  
38 Cavinato, G., Cannata, A., Pauselli, C., and Barchi, M.R.: Seismic reflection profiles and subsurface geology of the  
39 area interested by the 2016-2017 earthquake sequence (Central Italy), in: *The 2016 Central Italy Seismic Sequence:*  
40 *Insights, implications and lessons learned*, *Tectonics*, 37, 1116-1137, <https://doi.org/10.1002/2017TC004915>, 2018.

1 Porreca, M., Fabbrizzi, A., Azzaro, S., Pucci, S., Del Rio, L., Pierantoni, P. P., Giorgetti, C., Roberts, G., Barchi,  
2 M.R.: 3D geological reconstruction of the M. Vettore seismogenic fault system (Central Apennines, Italy): Cross-  
3 cutting relationship with the M. Sibillini thrust, *Journal of Structural Geology*, 131, 103938,  
4 <https://doi.org/10.1016/j.jsg.2019.103938>, 2020.

5 Pousse-Beltran, L., Vassallo, R., Audemard, F., Jouanne, F., Oropeza, J., Garambois, S., and Aray, J.: Earthquake  
6 geology of the last millennium along the Boconó Fault, Venezuela, *Tectonophysics*, 747-748, 40-53,  
7 <https://doi.org/10.1016/j.tecto.2018.09.010>, 2018.

8 Pucci, S., Pizzimenti, L., Civico, R., Villani, F., Brunori, C.A., Pantosti, D.: High resolution morphometric analysis  
9 of the Cordone del Vettore normal fault scarp (2016 central Italy seismic sequence): Insights into age, earthquake  
10 recurrence and throw rates, *Geomorphology*, 388, <https://doi.org/10.1016/j.geomorph.2021.107784>, 2021.

11 Quitzow, H. W.: Der Deckenbau des Kalabrischen Massivs und seiner Rangebiete. Beitr. geol. Westl.  
12 Mediterrangebiete Abh. Ges. Wiss. Gottingen, Math.-Phis. Kl. s. 3, 13: 63-179, 1935.

13 Reiss, S., Reicherter, K. R., and Reuther, C. D.: Visualization and characterization of active normal faults and  
14 associated sediments by high-resolution GPR Geological Society, London, Special Publications, 211, 247-255,  
15 doi:10.1144/GSL.SP.2001.211.01.20, 2003.

16 Roberts, G.P., Raithatha, B., Sileo, G., Pizzi, A., Pucci, S., Walker, J.F., et al.: Shallow subsurface structure of the  
17 2009 April 6 Mw 6.3 L'Aquila earthquake surface rupture at Paganica, investigated with ground-penetrating radar,  
18 *Geophys. J. Int.*, 183(2), 774-790, <https://doi.org/10.1111/j.1365-246X.2010.04713.x>, 2010.

19 Rovida, A., Locati, M., Camassi, R., Lolli, B., and Gasperini, P.: The Italian earthquake catalogue CPTI15, *Bulletin*  
20 *of Earthquake Engineering*, 18, 2953-2984, <https://doi.org/10.1007/s10518-020-00818-y>, 2020.

21 Salvi, S., Cinti, F.R., Colini, L., D'Addezio, G., Doumaz, F., and Pettinelli, E., Investigation of the active Celano-  
22 L'Aquila fault system, Abruzzi (central Apennines, Italy) with combined ground-penetrating radar and palaeoseismic  
23 trenching, *Geophys. J. Int.*, 155(3), 805-818, <https://doi.org/10.1111/j.1365-246X.2003.02078.x>, 2003.

24 Sangree, J., B. and Widmier, J. M.: Interpretation of depositional facies from seismic data, *Geophysics*, 44, 131-60,  
25 <https://doi.org/10.1190/1.1440957>, 1979.

26 Sapia, V., Villani, F., Fischanger, F., Lupi, M., Baccheschi, P., Pantosti, D., et al.: 3-D deep electrical resistivity  
27 tomography of the major basin related to the 2016 Mw 6.5 central Italy earthquake fault. *Tectonics*, 40,  
28 e2020TC006628, <https://doi.org/10.1029/2020TC006628>, 2021.

29 Schiattarella, M., Torrente, M., and Russo, F.: Analisi strutturale ed osservazioni morfotettoniche nel bacino del  
30 Mercure (Confine calabro-lucano), *Il Quaternario*, 7, 613-626, 1994.

31 Scognamiglio, L., Tinti, E., and Quintiliani, M.: Time Domain Moment Tensor (TDMT) [Data set], Istituto Nazionale  
32 di Geofisica e Vulcanologia (INGV), <https://doi.org/10.13127/TDMT>, <http://terremoti.ingv.it/tdmt>, 2006.

33 Servizio Geologico d'Italia: 220 Verbicaro and 221 Castrovillari Sheets of the Carta Geologica D'Italia, 1: 100.000  
34 Scale, Rome, 1970.

35 Shaikh, M.A., Maurya, D.M., Mukherjee, S., Vanik, N.P., Padmalal, A., and Chamyal, L.S.: Tectonic evolution of the  
36 intra-uplift Vigodi-Gugriana-Khirsara-Netra Fault System in the seismically active Kachhh rift basin, India:  
37 Implications for the western continental margin of the Indian plate, *Journal of Structural Geology*, 140, 104124,  
38 <https://doi.org/10.1016/j.jsg.2020.104124>, 2020.

39 Sketsiou, P., De Siena, L., Gabrielli, S., Napolitano, F., 3-D attenuation image of fluid storage and tectonic interactions  
40 across the Pollino fault network, *Geophysical Journal International*, 226:1, 536-547,  
41 <https://doi.org/10.1093/gji/ggab109>

1 Slater, L. and Niemi, T.M.: Ground-penetrating radar investigation of active faults along the Dead Sea Transform and  
2 implications for seismic hazards within the city of Aqaba, Jordan, *Tectonophysics*, 368(1-4), 33-50,  
3 [https://doi.org/10.1016/S0040-1951\(03\)00149-5](https://doi.org/10.1016/S0040-1951(03)00149-5), 2003.

4 Smith, D. G. and Jol, H. M.: Wasatch fault (Utah), detected and displacement characterized by ground penetrating  
5 radar, *Environ. Eng. Geosci.*, 1, 489-496, 1995.

6 Spina, V., Galli, P., Tondi, E., and Mazzoli, S.: Fault propagation in a seismic gap area (northern Calabria, Italy):  
7 implications for seismic hazard, *Tectonophysics*, 476, 357-369, 2009.

8 Stirling, M., Goded, T., Berryman, K., and Litchfield, N.: Selection of Earthquake Scaling Relationships for Seismic-  
9 Hazard Analysis, *Bulletin of the Seismological Society of America*, 103(6), 2993-  
10 3011, <https://doi.org/10.1785/0120130052>, 2013.

11 Tangari, A.C., Scarciglia, F., Piluso, E., Marinangeli, L., and Pompilio, L.: Role of weathering of pillow basalt,  
12 pyroclastic input and geomorphic processes on the genesis of the Monte Cerviero upland soils (Calabria, Italy), *Catena*,  
13 171, 299-315, ISSN 0341-8162, <https://doi.org/10.1016/j.catena.2018.07.015>, 2018.

14 Tarquini, S., Vinci, S., Favalli, M., Doumaz, F., Fornaciai, A. and Nannipieri, L.: Release of a 10-m-resolution DEM  
15 for the Italian territory: Comparison with global-coverage DEMs and anaglyph-mode exploration via the web,  
16 *Computers & Geosciences*, 38, 168-170, <https://doi.org/10.1016/j.cageo.2011.04.018>, 2012.

17 Tertulliani A. and Cucci, L.: New insights on the strongest historical earthquake in the Pollino region (southern Italy),  
18 *Seismol. Res. Lett.*, 85(3), 743-751, <https://doi.org/10.1785/0220130217>, 2014.

19 Testa, A., Boncio, P., Di Donato, M., Mataloni, G., Brozzetti, F., and Cirillo, D.: Mapping the geology of the 2016  
20 Central Italy earthquake fault (Mt. Vettore – Mt. Bove fault, Sibillini Mts.): geological details on the Cupi – Ussita  
21 and Mt. Bove - Mt. Porche segments and overall pattern of coseismic surface faulting, *Geological Field Trips and*  
22 *Maps, Italian Geological Society and of the Geological Survey of Italy*, 11(2.1), 1-13,  
23 <https://doi.org/10.3301/GFT.2019.03>, 2019.

24 Tortorici, L., Monaco, C., Tansi, C., and Cocina, O.: Recent and active tectonics in the Calabrian arc (Southern Italy),  
25 *Tectonophysics*, 243(1-2), pp. 37–55, [https://doi.org/10.1016/0040-1951\(94\)00190-K](https://doi.org/10.1016/0040-1951(94)00190-K), 1995.

26 Totaro, C., Koulakov, I., Orecchio, B., and Presti, D.: Detailed crustal structure in the area of the southern Apennines–  
27 Calabrian Arc border from local earthquake tomography, *J. Geodyn.*, 82, 87-97,  
28 <https://doi.org/10.1016/j.jog.2014.07.004>, 2014.

29 Totaro, C., Seeber, L., Waldhauser, F., Steckler, M., Gervasi, A., Guerra, I., Orecchio, B., and Presti, D.: An intense  
30 earthquake swarm in the southernmost Apennines: fault architecture from high-resolution hypocenters and focal  
31 mechanisms, *Bull. Seismol. Soc. Am.* 105, 1-6, <https://doi.org/10.1785/0120150074>, 2015.

32 Troncke, J., Villamor, P., and Green, A. G.: Detailed shallow geometry and vertical displacement estimates of the  
33 Maleme Fault Zone, New Zealand, using 2D and 3D georadar, *Near Surface Geophysics*, 4(3), 155-161,  
34 <https://doi.org/10.3997/1873-0604.2005041>, 2006.

35 Utzi, E. C.: *Ground Penetrating Radar*, Elsevier, 209 pp., <http://dx.doi.org/10.1016/B978-0-08-102216-0.00001-1>,  
36 2017.

37 Wallace, S. C., Nobes, D. C., Davis, K. J., Burbank, D. W., and White, A.: Three-dimensional GPR imaging of the  
38 Benmore anticline and step-over of the Ostler Fault, South Island, New Zealand, *Geophysical Journal International*,  
39 180(2), 465-474, <https://doi.org/10.1111/j.1365-246X.2009.04400.x>, 2010.

1 Vanneste, K., Verbeeck, K., and Petermans, T.: Pseudo-3-D imaging of a low-slip-rate, active normal fault using  
2 shallow geophysical methods: the Geleen fault in the Belgian Mass River valley, *Geophysics*, 73(1), B1–B9,  
3 <https://doi.org/10.1190/1.2816428>, 2008.

4 Wells, D.L. and Coppersmith, K.J.: New empirical relationships among magnitude, rupture length, rupture width,  
5 rupture area, and surface displacement, *Bull. Seismol. Soc. Am.*, 84(4), 974-1002, 1994.

6 Wesnousky, S.G.: Displacement and geometrical characteristics of earthquake surface ruptures: Issues and  
7 implications for seismic hazard analysis and the process of earthquake rupture, *Bull. Seismol. Soc. Am.*, 98(4), 1609-  
8 1632, <https://doi.org/10.1785/0120070111>, 2008.

9 Vezzani, L., Festa, A., and Ghisetti, F.C.: Geology and tectonic evolution of the Central-Southern Apennines, Italy,  
10 *Special Paper of the Geological Society of America*, 469, 1-58, <https://doi.org/10.1130/SPE469>, 2010.

11 Villani, F. and Pierdominici, S.: Late Quaternary tectonics of the Vallo di Diano basin (southern Apennines, Italy),  
12 *Quat. Sci. Rev.*, 29, 3167-3183, <https://doi.org/10.1016/j.quascirev.2010.07.003>, 2010.

13 Villani, F., Pucci, S., Civico, R., De Martini, P. M., Cinti, F. R., and Pantosti, D.: Surface faulting of the 30 October  
14 2016 Mw 6.5 central Italy earthquake: Detailed analysis of a complex coseismic rupture, *Tectonics*, 37, 3378-3410,  
15 <https://doi.org/10.1029/2018TC005175>, 2018.

16 Villani, F., Maraio, S., Bruno, P. P., Improta, L., Wood, K., Pucci, S., et al.: High-resolution seismic profiling in the  
17 hanging wall of the southern fault section ruptured during the 2016 Mw 6.5 central Italy earthquake. *Tectonics*, 40,  
18 e2021TC006786, <https://doi.org/10.1029/2021TC006786>, 2021.

19 Yalciner, C.C., Altunel, E., Bano, M., Meghraoui, M., Karabacak, V., and Akyuz, H. S.: Application of GPR to normal  
20 faults in the Büyük Menderes Graben, Western Turkey, *Journal of Geodynamics*, 65, 218-227,  
21 <https://doi.org/10.1016/j.jog.2012.05.011>, 2013.

22 Zajc, M., Celarc, B., and Gosar, A.: GPR Study of a Thrust-Fault in an Active Limestone Quarry (SW Slovenia),  
23 *JEEG*, 23(4), 457-468: <https://doi.org/10.2113/JEEG23.4.457>, 2018.

24 Zhang, D., Li, J., Liu, S., and Wang, G.: Multi-frequencies GPR measurements for delineating the shallow subsurface  
25 features of the Yushu strike slip fault, *Acta Geophys.*, 67, 501-515, <https://doi.org/10.1007/s11600-019-00271-9>,  
26 2019.

1

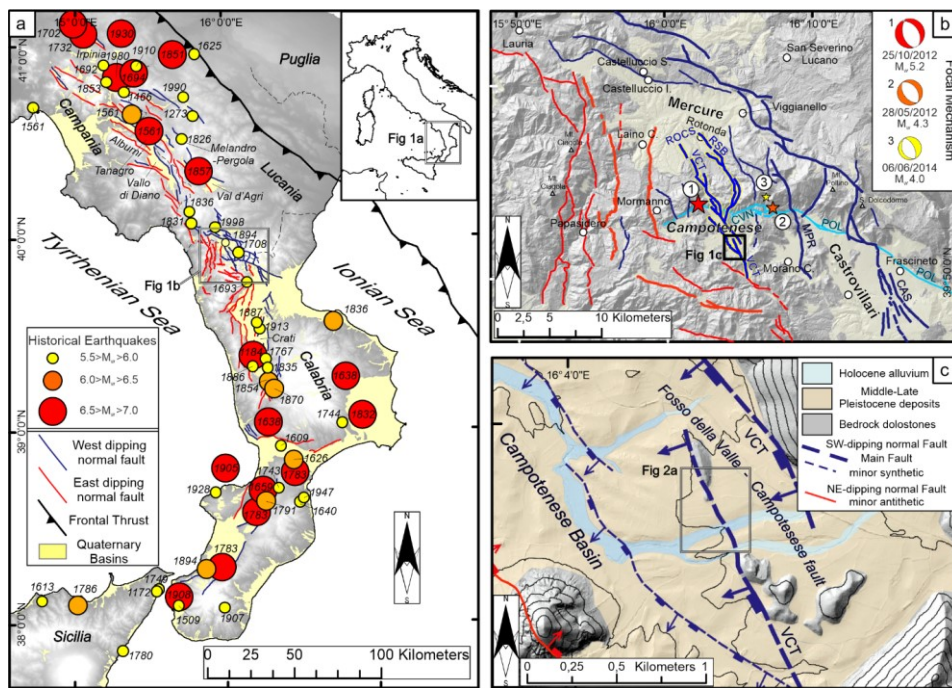


Figure 1

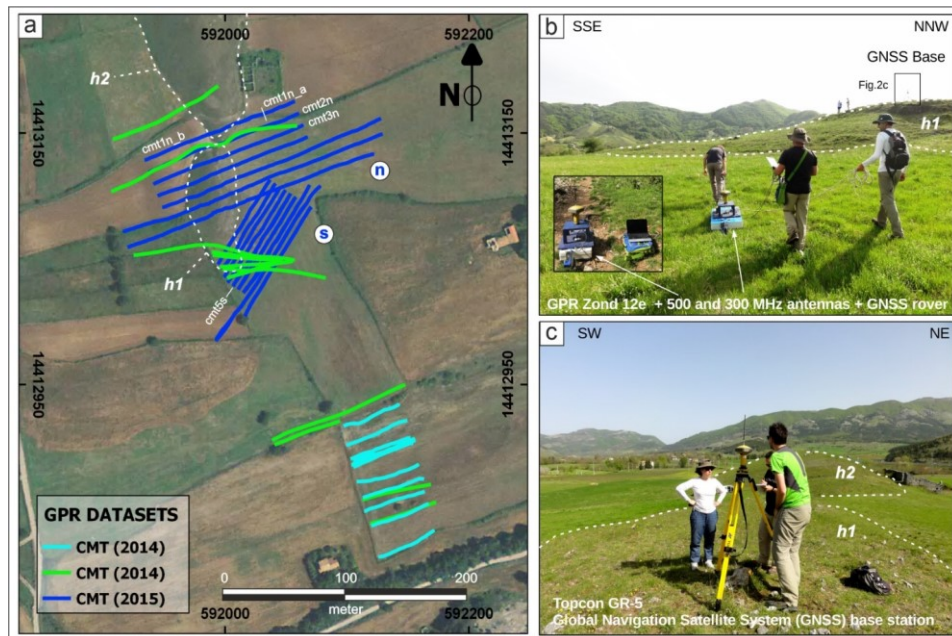


Figure 2



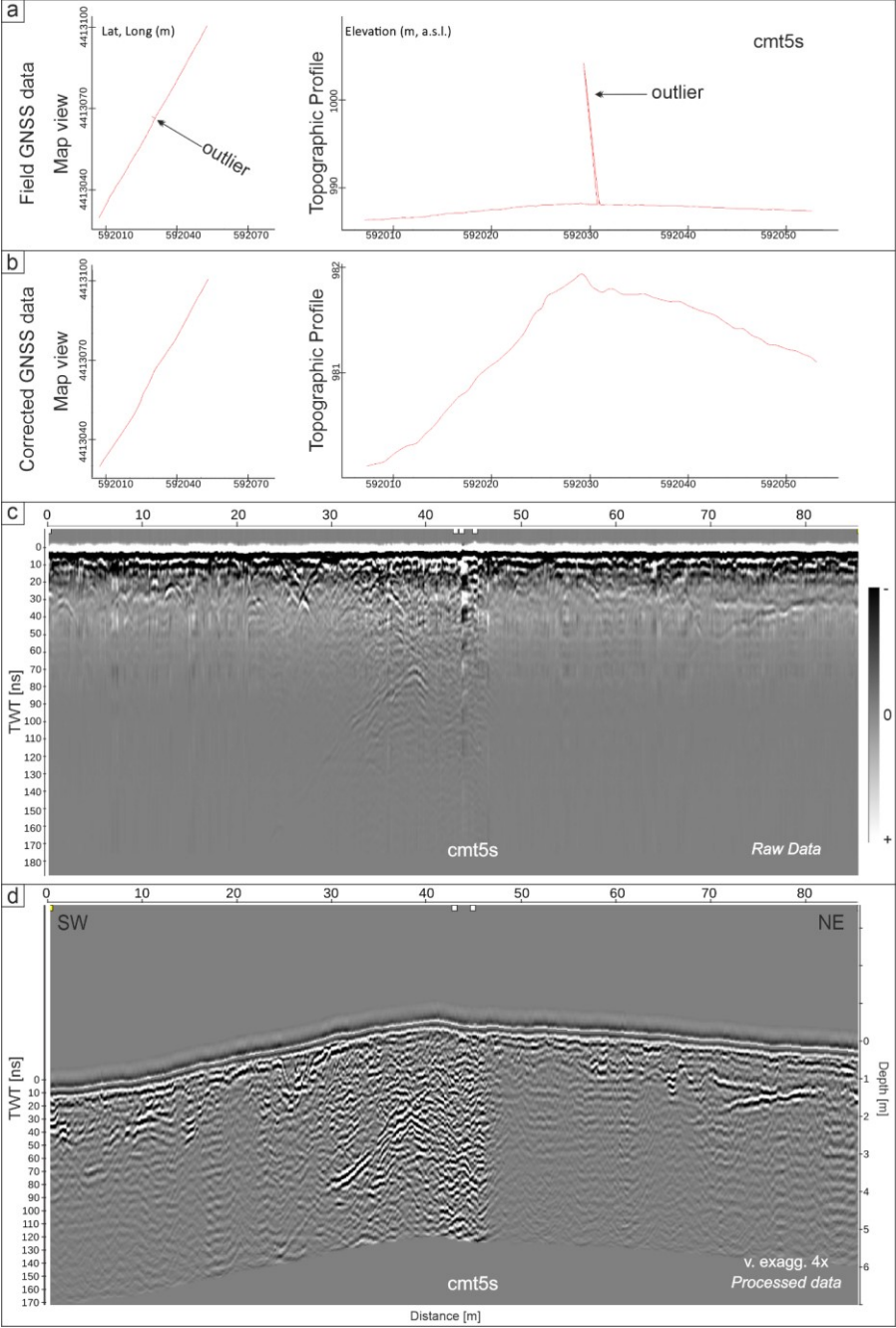
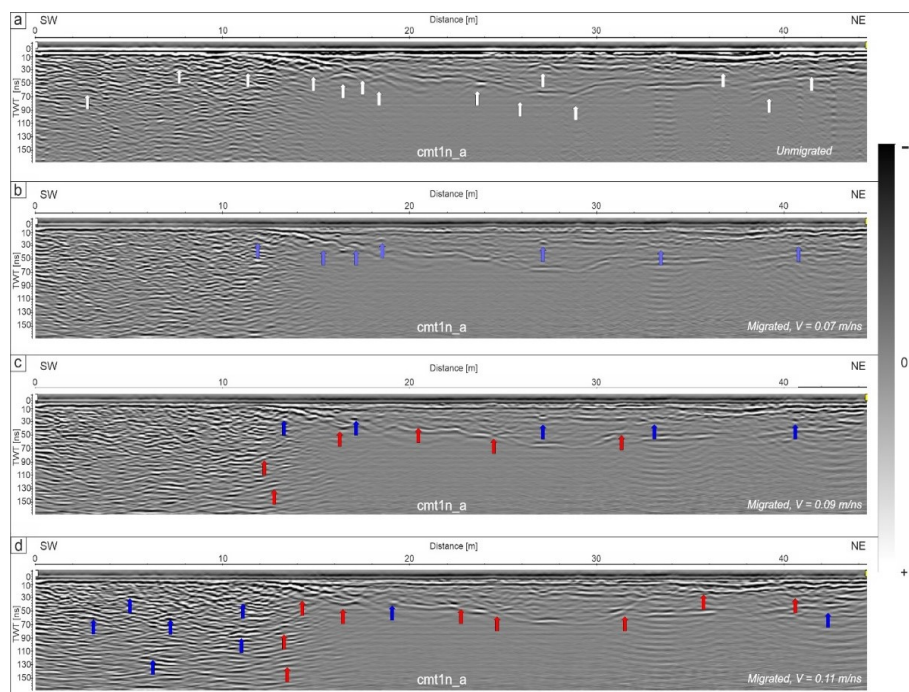
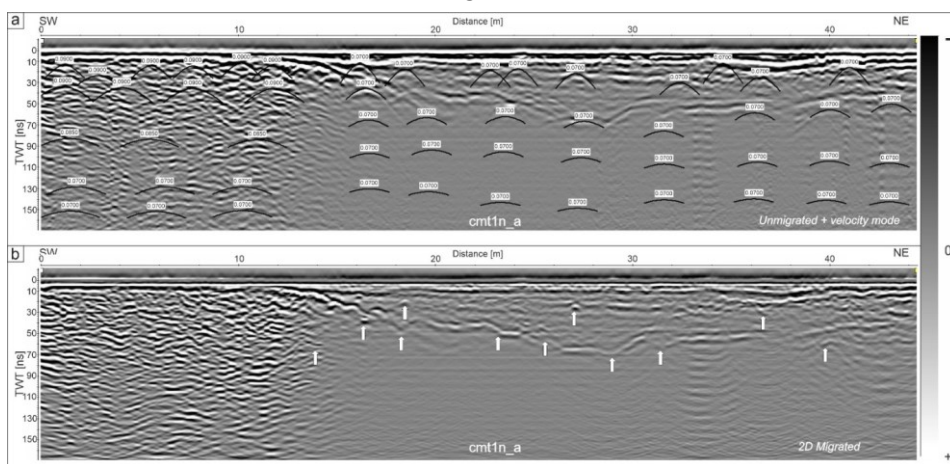


Figure 3



**Figure 4**



**Figure 5**

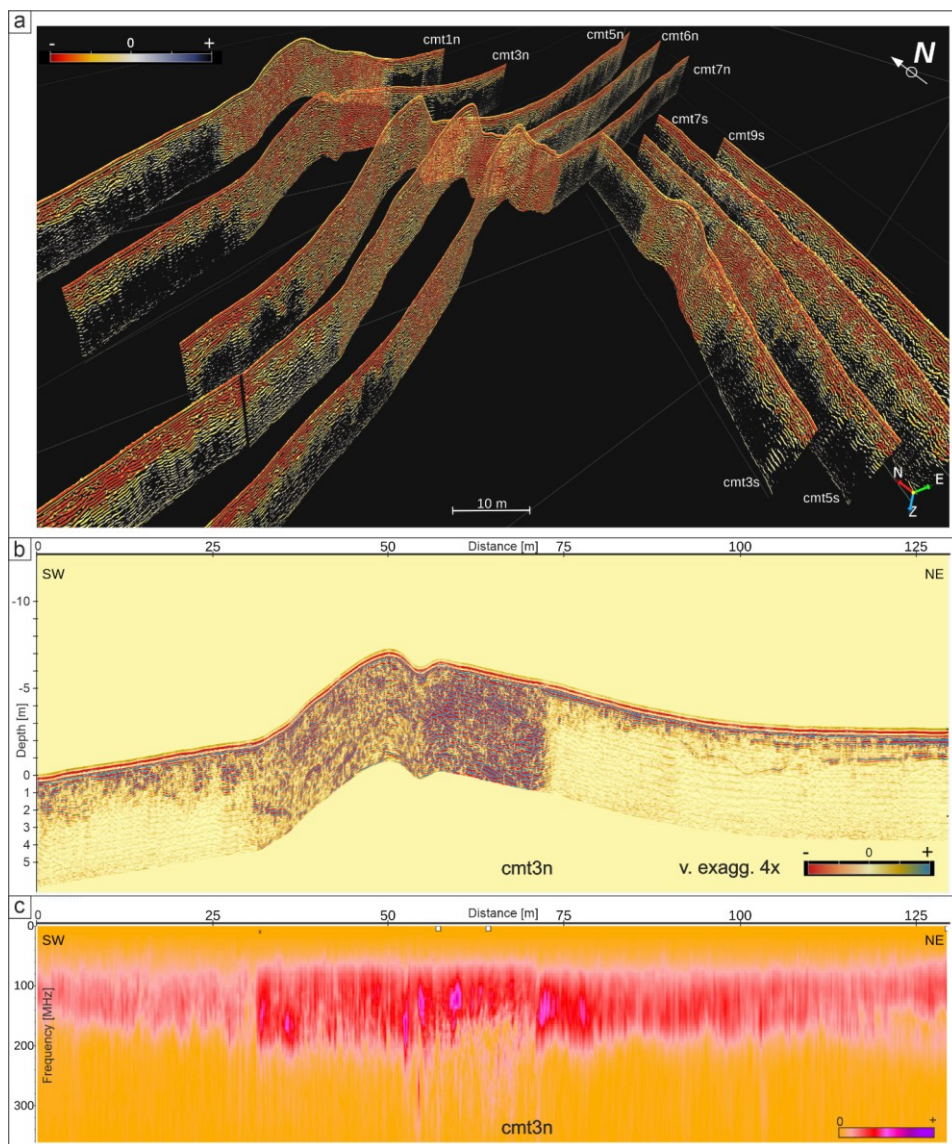


Figure 6



1

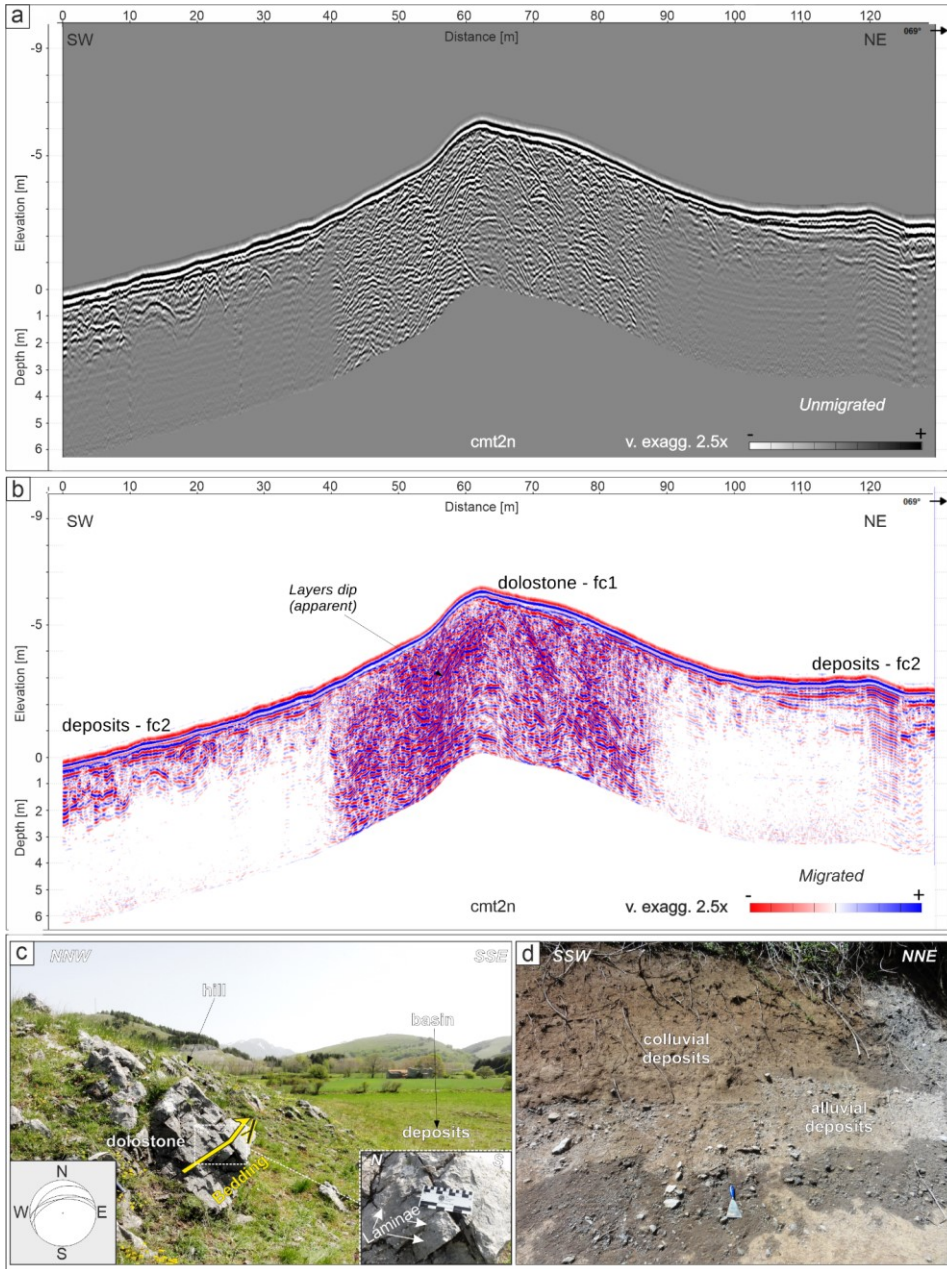


Figure 7

2

3

4

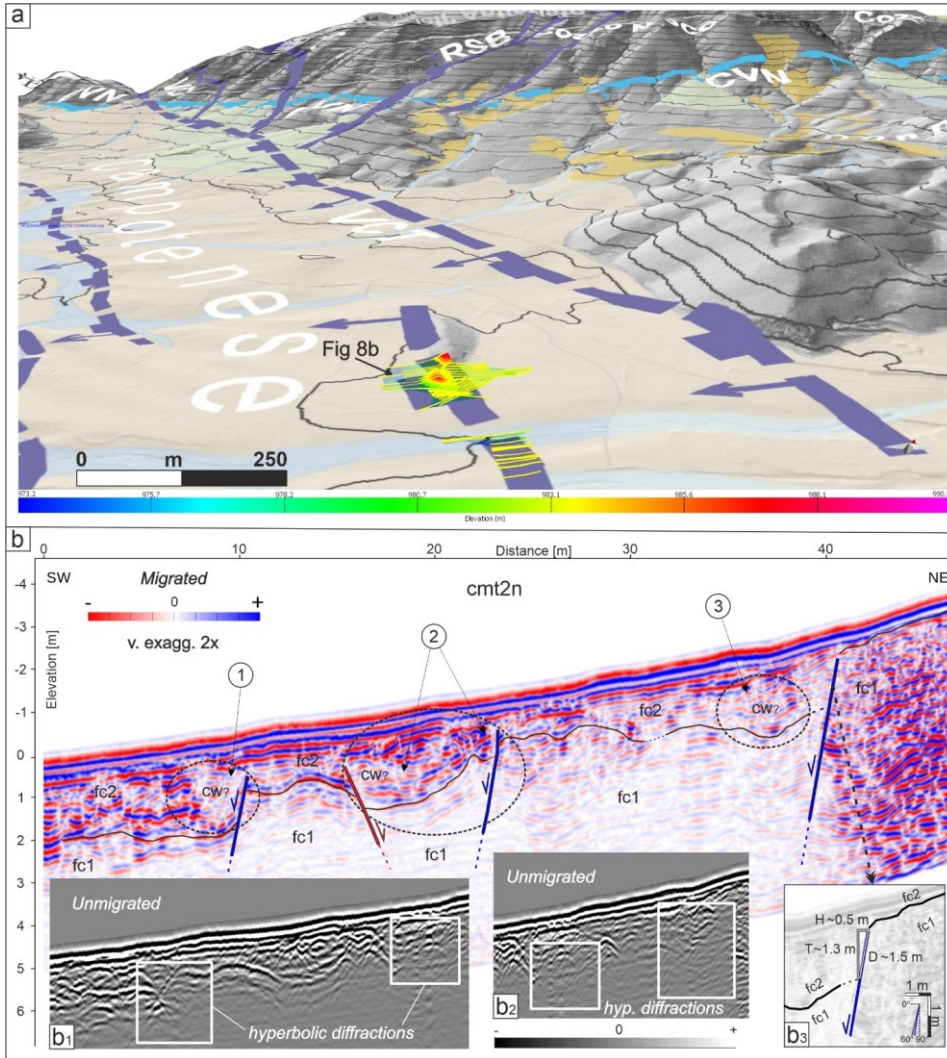


Figure 8

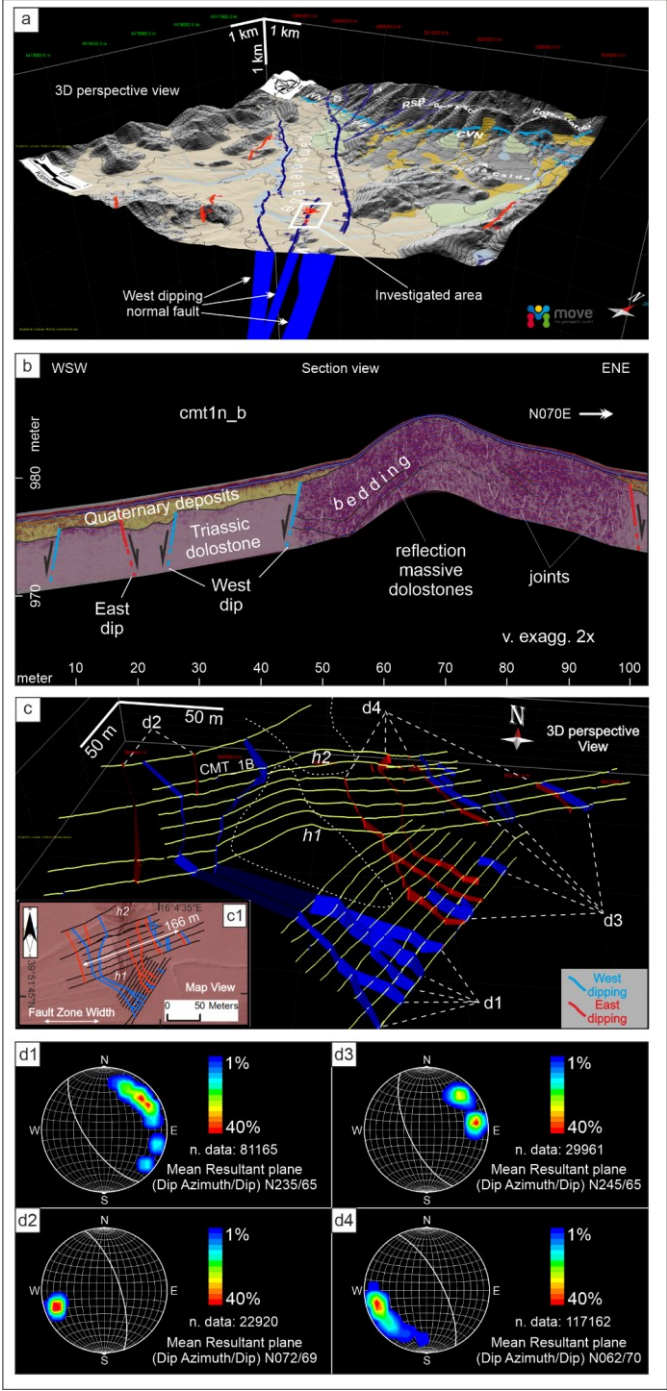


Figure 9

1

**Table 1**

GPR survey information and parameters		
Antenna frequency (MHz)	300 (preferred)	500
Number of acquired profiles	45	4
Total profile length (m)	3789.5/4153	363.5/4153
Profile distance (m)	10 and 25 (in g1 and g2)	not regular
Traces distance (m)	0.05	0.02
Number of samples	1024	512
Time window (ns)	300-200*	200-100*

2

3

**Table 2**

Processing Flow	Parameters (300 MHz)	Parameters (500 MHz)
Trace editing, coordinates editing and corrections	-	-
Time-zero correction	-	-
Dewow (ns)	10	5
Amplitude recovery function: $g(t)=(1+a*t)*e^{(b*t)}$	linear: 0.5 (2014) & 1.2 (2015) exponent: 0.15 (2014) & 0.6 (2015)	linear: 0.5 (2014) & 1.2 (2015) exponent: 0.15 (2014) & 0.6 (2015)
Velocity analysis	Diffraction hyperbola fittyng	Diffraction yperbola fitting
Background removal (ns)	Applied from 5 ns to end (computed on all the traces)	Applied from 5 ns to end (computed on all the traces)
Bandpass filter (MHz)	32/96/650/700	64/112/750/800
F-K filter	customized	customized
Time migration (2D Kirchhoff)	2D velocity models	2D velocity models
Topographic correction	GNSS/GIS Elevations	GNSS/GIS Elevations
Time-depth conversion (Quaternary deposits)	$v = 0,7 \text{ m/ns}$	$v = 0,7 \text{ m/ns}$

4

5



## Figures and Tables captions:

**Figure 1 - Location maps of the study site** (DTM sources: TINITALY by Tarquini et al., 2012 and by Regione Calabria - [www.regione.calabria.it](http://www.regione.calabria.it), under license IODL 2.0. - <https://www.dati.gov.it/iodl/2.0/>): a) the image illustrates the southern Italian peninsula with the regional faults pattern and the historical strong earthquakes (Rovida et al. 2020); b) map showing the studied region with local faults (modified after Brozzetti et al. 2017a), and epicenters (stars) and focal mechanisms of the mainshocks of the 2012-2014 seismic sequence (Scognamiglio et al., 2006); c) location of the GPR survey area within the Campotenese Quaternary basin crossing the Fosso della Valle - Campotenese (VCT) fault.

**Figure 2 - GPR acquisition campaigns:** a) GPR profiles collected at the study site Campotenese (“cmt”, where “n” and “s” stay for North and South, “h1” and “h2” indicate the two Dolostone hills outcropping in the basin) during the three field visits (aerial image source: Regione Calabria - [www.regione.calabria.it](http://www.regione.calabria.it), under license IODL 2.0. - <https://www.dati.gov.it/iodl/2.0/>); b) acquisition phase using the 300 and 500 MHz antennae (in the insert) and GNSS receivers used for accurate data positioning; c) GNSS base station set up during the fieldwork.

**Figure 3: Topographic correction of GPR profiles:** a) example of accuracy degradation of GNSS data, displaying an outlier both in map view and in topographic profile, on which the positioning error is considerable; b) GNSS coordinates and topographic profile after the correction; c) raw GPR section displaying high reflectivity in the central sector; d) example of full processed profile with topography displaying various reflection patterns encompassing dipping reflections and diffractions. Vertical exaggeration is 4.

**Figure 4: Migration tests performed during the GPR data processing:** a) unmigrated 2D GPR profile, 300 MHz antennae, displaying hyperbolic diffractions (white arrows); b) migrated profile using a constant velocity  $v = 0.07$  m/ns, light-blue arrows indicate good diffractions collapse; c) migration output obtained with a constant velocity  $v = 0.09$  m/ns, with dark-blue arrows suggesting good migration results (migration artefacts are shown by red arrows); d) migration results using a constant velocity  $v = 0.11$  m/ns, with dark-blue arrows highlighting good hyperbolas collapse, particularly within the high reflective unit; red arrows highlight clear migration smiles.

**Figure 5: Example of 2D time-migration of radar profiles:** a) example of hyperbolic diffractions fitting used for 2D velocity model building; a constant velocity value (0.07 m/ns) was assumed in deeper no-diffraction areas for interpolation purposes; b) 2D time-migration results, highlighting the good performance of the process, which collapsed the hyperbolic diffractions (white arrows) and restored reliable reflection geometry.

**Figure 6: GPR data visualization:** a) fence diagram showing the three-dimensional location of some representative GPR profiles in the northern sector of the study site; b) bidimensional GPR profile (cmt3n, see figure 2a for location) displaying the central high reflective sector and dipping reflections across the hill; c) spatial variation of a 2D amplitude-frequency spectrum linked to variable physical properties of media along the profile cmt3n. Vertical exaggeration is 4.

**Figure 7: Correlation between GPR profiles and outcropping geology at the study site:** a) unmigrated 300 MHz profile (cmt2n, see fig. 2b for location) displaying numerous hyperbolic diffractions; b) migrated profile displaying the apparent dip associated to fractured dolostone formation (facies fc1) and Quaternary deposits in the attenuated sectors (GPR facies fc2); c) Quaternary deposits of the basin (on the background) surrounding the Triassic Dolostone formation outcropping on the hill h1. The yellow arrows indicate the bedding, such as the stereo-net (left-side inset); the right-side inset report a detail of the laminae visible on site and nearby; d) an example of Quaternary colluvial and alluvial deposits outcropping nearby the survey site. Vertical exaggeration is 2.5.

**Figure 8: GPR data interpretation:** a) three-dimensional image of the surveyed area (see fig. 1c for location), displaying the Dolostone outcrops (grey colour). Blue dashed lines are the VCT and RSB faults (fig. 1b), whilst the light blue is CVN fault. In yellow lines the GPR profiles; the coloured surface is the interpreted Dolostone top reflection (DTM source: Regione Calabria - [www.regione.calabria.it](http://www.regione.calabria.it), under license IODL 2.0. - <https://www.dati.gov.it/iodl/2.0/>); b) migrated radar profile with the main interpreted normal faults (blue and red are W- and E- dipping structures, respectively) as well as related sedimentary structures within the Quaternary deposits (unmigrated data in b1 and b2); the inset b3 is a schematic representation illustrating the methodology used for extraction of the GPR fault displacement (D: displacement; T: throw; H: heave). GPR facies fc2 shows semi-continuous and sub-horizontal reflections (Quaternary deposits) onlapping fc1 (Triassic Dolostones, black line is the “top”). In circle 1: reflections package thickening and truncation with localized attenuation are likely interpretable as “colluvial-wedge-like” (cw?) features, or deposits from degradation of earthquake fault free-face nearby of the hanging-wall ( $D \sim 0.6$  m). In circle 2: fc2 show more discontinuous, from subparallel to wavy reflections package downlapping the lower top Dolostone; the

Deleted:

1 asymmetric, truncated reflections thickening is bounded by two conjugate normal fault strands (east dip  $D \sim$   
2  $0.5$  m, west-dip  $D = 0.4$  m) displacing both  $fc1$  and  $fc2$ . In circle 3: contorted reflections package with limited  
3 continuity, displaying thickening, truncation and distributed attenuation, suggesting colluvial wedge deposits  
4 close to the main fault zone ( $D \sim 1.5$  m, inset b3). Vertical exaggeration is 2.

5 **Figure 9:** Results of the three-dimensional analysis and interpretation performed on the entire GPR dataset:  
6 a) 3D structural model of the Campotenese basin updated after Brozzetti et al., 2017a (DTM sources:  
7 TINITALY by Tarquini et al., 2012 and by Regione Calabria - [www.regione.calabria.it](http://www.regione.calabria.it), under license IODL  
8 2.0. - <https://www.dati.gov.it/iodl/2.0/>); b) GPR section view (cmtIn-b) with interpretation including synthetic  
9 and antithetic fault splays (blue= W-to SW-dip; red=E-to NE-dip, respectively); c) detailed structural scratch  
10 of faults obtained by the analysis and correlation of interpreted fault slapys across the entire GPR dataset; the  
11 inset c1 is a conventional structural map oriented to the North and reporting the same fault sets to highlight  
12 the maximum width derived for the fault zone d) synthetic stereo-net plots of the fault planes in c), reporting  
13 the mean Dip Azimuth / Dip angle extracted for the identified four main sets of discontinuities, with a Dip  
14 Azimuth ranging between  $N\ 235-245^\circ$  and  $N\ 062-072^\circ$  for the W-dipping and E-dipping normal faults,  
15 respectively. Vertical exaggeration is 2.

16 **Table 1:** Main information and GPR parameters used during the data collection (\* the time window was  
17 adapted depending on the surveyed area).

18 **Table 2:** Customized flow and details of the parameters used during the processing of the GPR dataset.